https://doi.org/10.1093/plcell/koad215 THE PLANT CELL 2023: 35: 4066–4090

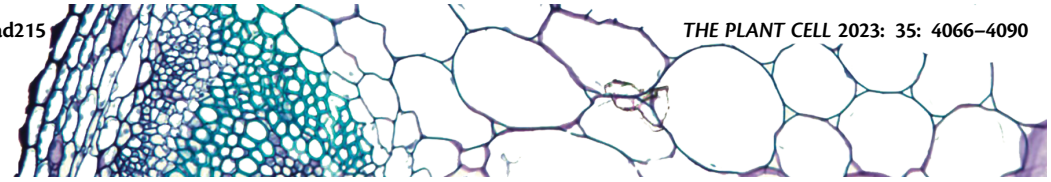

Research Article

The transcription factors ZmNAC128 and ZmNAC130 coordinate with Opaque2 to promote endosperm filling in maize

Erwang Chen [1,†] Huiqin Yu [1,†] Juan He [1,†] Di Peng [1,†] Panpan Zhu [1] Shuxing Pan [1] Xu Wu [1] Jincang Wang [1] Chen Ji [2] Zhenfei Chao [2] Zhuopin Xu [3] Yuejin Wu [3] Daiyin Chao [2] Yongrui Wu [2] and Zhiyong Zhang [1,*,‡]

1 School of Life Sciences, Division of Life Sciences and Medicine, University of Science and Technology of China, Hefei 230027, China
2 National Key Laboratory of Plant Molecular Genetics, CAS Center for Excellence in Molecular Plant Sciences, Shanghai Institute of Plant Physiology and Ecology, Chinese Academy of Sciences, Shanghai 200032, China
3 Anhui Key Laboratory of Environmental Toxicology and Pollution Control Technology, Hefei Institutes of Physical Science, Chinese Academy of Sciences, Hefei, Anhui 230031, China

*Author for correspondence: zhiyong2@ustc.edu.cn (Z. Z.)
†These authors contributed equally to this work.
‡Senior author.
The author responsible for distribution of materials integral to the findings presented in this article in accordance with the policy described in the Instructions for Authors (https://academic.oup.com/plcell/pages/General-Instructions) is: Zhiyong Zhang (zhiyong2@ustc.edu.cn).

Abstract

Endosperm filling in maize (*Zea mays*), which involves nutrient uptake and biosynthesis of storage reserves, largely determines grain yield and quality. However, much remains unclear about the synchronization of these processes. Here, we comprehensively investigated the functions of duplicate NAM, ATAF1/2, and CUC2 (NAC)-type transcription factors, namely, ZmNAC128 and ZmNAC130, in endosperm filling. The gene-edited double mutant *zmnac128 zmnac130* exhibits a poorly filled kernel phenotype such that the kernels have an inner cavity. RNA sequencing and protein abundance analysis revealed that the expression of many genes involved in the biosynthesis of zein and starch is reduced in the filling endosperm of *zmnac128 zmnac130*. Further, DNA affinity purification and sequencing combined with chromatin-immunoprecipitation quantitative PCR and promoter transactivation assays demonstrated that ZmNAC128 and ZmNAC130 are direct regulators of 3 (*16-*, *27-*, and *50-kD*) *γ-zein* genes and 6 important starch metabolism genes (*Brittle2* [*Bt2*], *pullulanase-type starch debranching enzyme* [*Zpu1*], *granule-bound starch synthase 1* [*GBSS1*], *starch synthase 1* [*SS1*], *starch synthase IIa* [*SSIIa*], and *sucrose synthase 1* [*Sus1*]). ZmNAC128 and ZmNAC130 recognize an additional cis-element in the *Opaque2* (*O2*) promoter to regulate its expression. The triple mutant *zmnac128 zmnac130 o2* exhibits extremely poor endosperm filling, which results in more than 70% of kernel weight loss. ZmNAC128 and ZmNAC130 regulate the expression of the transporter genes *sugars that will eventually be exported transporter 4c* (*ZmSWEET4c*), *sucrose and glucose carrier 1* (*ZmSUGCAR1*), and *yellow stripe-like2* (*ZmYSL2*) and in turn facilitate nutrient uptake, while O2 plays a supporting role. In conclusion, ZmNAC128 and ZmNAC130 cooperate with O2 to facilitate endosperm filling, which involves nutrient uptake in the basal endosperm transfer layer (BETL) and the synthesis of zeins and starch in the starchy endosperm (SE).

Received March 13, 2023. Accepted July 12, 2023. Advance access publication August 5, 2023

IN A NUTSHELL

Background: Cereal endosperms store starch and proteins in grains and play a critical role in determining grain yield and quality. Maize (*Zea mays*), with its sizable grain, is an excellent model for studying cereal endosperm development. Endosperm filling involves 2 synchronized processes: maternal-to-endosperm nutrient transfer and storage reserve biosynthesis. Several important nutrient transfer-related genes have been identified, and the regulation of storage reserve biosynthesis has been broadly studied in maize. Notably, the transcription factor-encoding genes *Opaque2* (*O2*), *ZmNAC128*, and *ZmNAC130* exhibit strong expression in the filling endosperm. However, how these 3 transcription factors co-regulate the synchronization of these endosperm-filling processes remains elusive.

Question: What are the roles of ZmNAC128 and ZmNAC130 in endosperm filling? How do they function together with O2 in this process?

Findings: ZmNAC128 and ZmNAC130 directly regulate the expression of all *γ-zein* genes (encoding storage proteins) and multiple important starch metabolism genes, making them pivotal coordinators of grain quality and yield. Furthermore, ZmNAC128 and ZmNAC130 directly regulate the expression of *O2*, and together these 3 transcription factors synergistically activate their expression through autoregulation and physical interactions. ZmNAC128 and ZmNAC130 also regulate the expression of vital transporter genes responsible for facilitating nutrient transfer from the mother plant to the endosperm. This regulatory mechanism enhances nutrient uptake, with O2 playing a supportive role.

Next steps: We plan to identify additional co-regulatory factors involved in endosperm filling to gain a comprehensive understanding of endosperm filling, from nutrient uptake to the biosynthesis of storage reserves.

Introduction

Cereal grain endosperms, which serve as the main storage site of starch and proteins in kernels, account for approximately 90% of kernel weight (Flint-Garcia et al. 2009). The endosperm supports embryogenesis and seed germination during early seedling development, while the endosperm is also a main source of food, feed, and industrial raw materials worldwide (Flint-Garcia 2017; Hannah and Boehlein 2017; Huang et al. 2021). Among cereals, maize (*Zea mays*) has the largest caryopsis, making it an excellent model species for investigating endosperm development (Sabelli and Larkins 2009). Like that of other cereal grains, maize endosperms start to develop after double fertilization, wherein one sperm fertilizes the diploid central cell to initiate the formation of the triploid endosperm (Sabelli and Larkins 2009).

Endosperm development involves 3 typical physiological stages: early, middle, and mature stages. During the early stage, the fertilized endosperm undergoes coenocyte formation, cellularization, and differentiation (Olsen 2001). Seven distinguishable compartments are formed approximately 8 d after pollination (DAP): starchy endosperm (SE), aleurone (AL), embryo surrounding region (ESR), basal endosperm transfer layer (BETL), basal-intermediate zone (BIZ), conducting zone (CZ), and subaleurone (SA) (Olsen 2001; Becraft and Gutierrez-Marcos 2012; Leroux et al. 2014; Zhan et al. 2017; Dai et al. 2021). Endosperm cell fate is largely determined during this stage. Starting at approximately 8–10 DAP, endosperm development is accompanied by the coordination of maternal-to-filial nutrient transfer in the BETL and the synthesis of storage reserves in the SE, which ultimately determine the yield and quality of the kernel. Subsequently, kernels gradually dehydrate and mature.

In recent years, spatiotemporal high-resolution transcriptome analyses and advanced functional genomic studies have greatly advanced our understanding of endosperm development in maize (Xin et al. 2013; Chen et al. 2014; Zhan et al. 2015; Yi et al. 2019; Li and Wu 2020). For instance, the BETL at the base of the endosperm is the gateway through which nutrients are transported to the central SE, a process that is facilitated by the BIZ and CZ compartments (Chourey and Hueros 2017). When mutated, BETL-specific sugar transfer-related genes including *Miniature1* (*ZmMN1*, encoding CELL WALL INVERTASE2) (Cheng et al. 1996), *Sugars will eventually be exported transporter 4c* (*ZmSWEET4c*) (Sosso et al. 2015), and *Sucrose and glucose carrier 1* (*ZmSUGCAR1*, also referred to as *ZmNPF7.9* [*Nrt1/Ptr family 7.9*] and *ZmMN2*) largely block mother-to-endosperm sugar transfer and the synthesis of storage reserves (Guan et al. 2020; Wei et al. 2021; Zhou et al. 2021; Yang et al. 2022a). Recently, the *shrunken4* (*sh4*) mutant was shown to harbor a mutation in the oligopeptide metal transporter YELLOW STRIPE-LIKE2 (ZmYSL2), which predominantly exists in the AL and BETL compartments (He et al. 2021; Chao et al. 2022). Like mutants with defects in sugar transporter genes expressed in the BETL, the *sh4* mutant also exhibits a shrunken-kernel phenotype, suggesting that ZmYSL2 is critical for endosperm filling. MYB-RELATED PROTEIN1 (MRP1) is an important transcription factor (TF) for BETL development and function (Gomez et al. 2002; Gomez et al. 2009); loss-of-function mutants are needed to determine its role during grain filling.

The SE compartment occupies the largest part of the endosperm and is the site of the biosynthesis and deposition of

storage reserves during the filling stage. Ultramicroscopy observations of filling-stage and mature endosperms revealed that the SE is filled with 2 types of storage bodies: starch granules (SGs) and protein bodies (PBs) (Sabelli and Larkins 2009). SGs are formed by the orderly assembly of starch in amyloplasts (Hannah and Boehlein 2017). Starch accounts for approximately 70% of dry kernel weight, so its content is closely related to yield. PBs, which are insoluble and spherical, are formed by the synthesis and deposition of zeins (the most abundant seed storage proteins in maize) within the lumen of the rough endoplasmic reticulum (Lending and Larkins 1989; Larkins et al. 2017). Zeins lack several essential amino acids (lysine, tryptophan, and methionine), which greatly affects seed protein quality (Larkins et al. 2017). Temporal high-resolution transcriptome analyses of endosperm development have indicated that genes encoding zeins and enzymes participating in starch biosynthesis are specifically and strongly expressed during the filling stage (Chen et al. 2014). This suggested that common TFs or regulators might contribute to their synchronized biosynthesis.

The first TF identified related to zein biosynthesis was Opaque2 (O2), which directly regulates the expression of *22-kD α-zein* through the recognition of the O2-box cis-element in its promoter (Schmidt et al. 1987; Schmidt et al. 1990). Analysis of differentially expressed genes (DEGs) in the *o2* mutant, combined with genome-wide chromatin-immunoprecipitation followed by deep sequencing (ChIP-seq), revealed that O2 regulates the expression of most zein genes, with the exception of the *16-kD γ-zein* gene (Li et al. 2015; Zhan et al. 2018). ZmNAC128 and ZmNAC130 were recently shown to regulate the expression of *16-kD γ-zein* via their ability to bind to a specific cis-element (ACGCAA) in its promoter (Zhang et al. 2019), although it remains unknown whether or how these 2 NAM, ATAF1/2, and CUC2s (NACs) regulate the expression of other zein genes. The 27-kD γ-zein is involved in the initiation of PB formation (Wu et al. 2010), and its expression is regulated by a complex series of TFs, including BASIC LEUCINE ZIPPER22 (ZmbZIP22) (Li et al. 2018), PROLAMIN-BOX BINDING FACTOR1 (PBF1) (VicenteCarbajosa et al. 1997; Wu and Messing 2012), O2 HETERODIMERIZING PROTEINS (OHP1 and OHP2) (Pysh et al. 1993; Zhang et al. 2015), and O2 (Li et al. 2015). Upon the interaction with O2, ZmMADS47, a MADS box-containing TF, binds to the CATGT (short sequence of five nucleotides) motif in the promoters of *α-zein* and *50-kD γ-zein* for their transactivation (Qiao et al. 2016). In general, O2 appears to be a core TF that regulates the expression of zein genes through additive and synergistic interactions with multiple TFs, including ZmbZIP22, PBF1, OHP1, OHP2, and ZmMADS47.

Among the characterized TFs regulating the expression of zein genes, some also directly regulate the expression of genes encoding enzymes in the starch biosynthesis pathway. Our previous studies demonstrated that O2 coordinates the expression of important starch metabolism genes, including *starch synthase III* (*SSIII*), the 3 major sucrose synthases (*sucrose synthase Sh1* [*Shrunken1*], *sucrose synthase 1* [*Sus1*], and *Sus2*), and *pyruvate orthophosphate dikinase* (*PPDK*) (Zhang et al. 2016; Deng et al. 2020). Knockdown of *ZmNAC128* and *ZmNAC130* via RNA interference (RNAi) significantly downregulated the expression of multiple starch metabolism genes. Among these genes, *Brittle2* (*Bt2*), which encodes the adenosine diphosphate glucose pyrophosphorylase (AGPase) small subunit, is a direct downstream target of ZmNAC128 and ZmNAC130 (Zhang et al. 2019).

Although ZmNAC128 and ZmNAC130 are also important coordinators of the synchronized synthesis of zeins and starch, their gene regulatory networks (GRN) remain largely unknown. Additionally, Opaque11 (O11), a hub TF for endosperm development, also directly regulates the expression of carbohydrate-related genes (*starch synthase V* [*SSV*] and *pyruvate kinase*) (Feng et al. 2018). Moreover, NAKED ENDOSPERM1 (NKD1) and NKD2 directly or indirectly regulate the expression of zein genes, and are also predicted to act as transcriptional activators of *starch synthase 1* (*SS1*), *sugary1* (*Su1*), and *waxy* (*Wx*) (Gontarek et al. 2016). We do not yet clearly understand the transcriptional regulation of starch metabolism genes in the endosperm. One way to fill this gap is to identify additional TFs that regulate starch metabolism via forward or reverse genetics; another complementary approach is to determine the GRN of the identified TFs, such as ZmNAC128 and ZmNAC130 or NKD1 and NKD2, by DEG analysis in their respective mutants combined with global cis-element characterization. Such an approach successfully revealed the GRN of O2 and PBF1 through the combined analysis of DEGs and genome-wide ChIP-seq by different groups (Li et al. 2015; Zhan et al. 2018; Ning et al. 2022).

In general, endosperm filling has been intensively investigated over the past few decades, and progress has been made in understanding the regulation of storage proteins and starch, nutrient transfer, and initiation of filling. However, the synchronization of these events during grain filling remains poorly understood. *O2*, *ZmNAC128*, and *ZmNAC130* are the most highly expressed TF-encoding genes in the filling-stage endosperm (Chen et al. 2014). O2 has been comprehensively investigated in recent decades, but ZmNAC128 and ZmNAC130 remain poorly understood. This study aims to shed light on the roles of ZmNAC128, ZmNAC130, and O2 in regulating endosperm filling. These roles encompass the coordination of zeins and starch synthesis, maintaining their high expression levels, and regulating the expression of critical transporter genes in the BETL.

Results

ZmNAC128 and ZmNAC130 are essential for endosperm filling

Our previous study found that knockdown of expression of *ZmNAC128* and *ZmNAC130* via RNA interference (RNAi)

caused a shrunken-kernel phenotype with 30% of kernel weight loss, while a *zmnac130* mutant of a 5-amino acids deletion within the conserved NAC domain of its encoding protein did not lead to any apparent kernel phenotype. Meanwhile, ZmNAC128 and ZmNAC130 could recognize the same cis-element ACGCAA to co-regulate the expression of *16-kD γ-zein* and *Bt2*, which suggests their functional redundancy (Zhang et al. 2019). However, the contribution of ZmNAC128 and ZmNAC130 to endosperm filling remains largely unknown.

Therefore, knockout mutants of *ZmNAC128* and *ZmNAC130* were generated by clustered regularly interspaced short palindromic repeats (CRISPR)/CRISPR-associated nuclease 9 (Cas9)-mediated gene editing in this study. We obtained 3 independent knockout mutants, each of which had a different frameshift mutation: *zmnac128-1*, *zmnac128-2*, *zmnac128-3*, *zmnac130-1*, *zmnac130-2*, and *zmnac130-3* (Supplemental Fig. S1). The 6 single mutants exhibited normal cob and kernel phenotypes similar to the wild-type (WT) KN5585. However, all double mutants of different allele combinations of *zmnac128* and *zmnac130* exhibited the same poorly filled-kernel phenotype (Supplemental Fig. S1). Among these knockout mutants, *zmnac128-1*, *zmnac130-1*, and *zmnac128-1 zmnac130-1*, which were abbreviated as *zmnac128*, *zmnac130*, and *zmnac128 zmnac130*, hereafter, were used for subsequent studies.

Observations of kernel longitudinal sections revealed a cavity within the endosperm of *zmnac128 zmnac130* and its peripheral endosperm became floury, while kernel phenotypes of the single mutants *zmnac128* and *zmnac130* were the same as that of the WT (Fig. 1A). Scanning electron microscopy (SEM) observations indicated that the SGs are smaller in the endosperm of *zmnac128 zmnac130* than in that of the WT (Fig. 1A). The hundred-kernel weight (HKW) of *zmnac128 zmnac130* was 56.8% lower than that of the WT, while the HKW of *zmnac128* and *zmnac130* was not significantly reduced (Fig. 1B). Although their RNAi mutants (*nacRNAi*) also caused 30% of kernel weight loss compared to the corresponding nontransgenic (NT) kernels (Zhang et al. 2019), it is obvious that knockout of *ZmNAC128* and *ZmNAC130* lead to even lower kernel weight and more severe kernel phenotypes than that of *nacRNAi*.

Furthermore, we analyzed the protein and starch contents in mature kernels via near-infrared (NIR) spectroscopy analysis (Fig. 1C). The starch contents in the kernels of the 2 single mutants were slightly but significantly reduced, while the protein content in the kernels of *zmnac128* was also slightly reduced with a significant difference. However, the contents of protein and starch in the kernels of *zmnac128 zmnac130* decreased by more than 50% compared to those of the WT and were also lower than those of *nacRNAi* (Zhang et al. 2019). Therefore, these knockout mutants generated in this study are a prerequisite for comprehensively investigating the function of ZmNAC128 and ZmNAC130 in the endosperm filling. These results clearly pointed out that ZmNAC128 and ZmNAC130 redundantly promote endosperm filling, as their simultaneous loss of function severely impaired the accumulation of storage reserves.

RNA-seq combined with DNA affinity purification-seq facilitates the functional dissection of ZmNAC128 and ZmNAC130

DEG analysis of zmnac128 zmnac130 indicates the enrichment of zein and starch metabolism

To study the GRN of ZmNAC128 and ZmNAC130, we conducted RNA sequencing (RNA-seq) analysis using total RNA extracted from 16-DAP endosperms of WT, *zmnac128*, *zmnac130*, and *zmnac128 zmnac130* in the KN5585 background. We identified DEGs in the 3 mutants relative to the WT based on the selection criteria of a fold-change (FC) ≥ 2 and a *P*-value ≤ 0.05. Only 80 and 2 DEGs were detected in *zmnac128* and *zmnac130*, respectively. However, this number rose to 2,686, with 1,529 upregulated and 1,157 downregulated genes in *zmnac128 zmnac130* (Fig. 2A and Supplemental Data Set 1). This result further supported the functional redundancy of the 2 NACs.

We performed an enrichment analysis of Gene Ontology (GO) terms and Kyoto Encyclopedia of Genes and Genomes (KEGG) pathways based on the DEGs in *zmnac128 zmnac130*. We observed 2 significantly enriched GO terms for molecular function, one of which was "nutrient reservoir activity" (GO:0045735, *P*-value = 2.17E−06), which mainly included zein family genes (Fig. 2B). Indeed, the expression of all zein family genes was significantly downregulated to varying extents in *zmnac128 zmnac130* (Supplemental Table S1). Moreover, multiple carbohydrate metabolism-related pathways were enriched (Fig. 2B). These results suggested that ZmNAC128 and ZmNAC130 play crucial roles in the biosynthesis of zeins and starch.

DNA affinity purification-seq reveals genome-wide binding features of ZmNAC128 and ZmNAC130

DNA affinity purification and sequencing (DAP-seq) is a recently developed method of genome-wide TF-binding site identification, which is fast, inexpensive, and more easily scaled than ChIP-seq and bypasses the difference of sampling stage (Bartlett et al. 2017; Galli et al. 2018). In this study, we conducted the DAP-seq assay by incubation of recombinant purified ZmNAC128 and ZmNAC130 proteins and the use of a DNA library prepared from genomic DNA extracted from 16-DAP endosperms of the reference inbred line B73. The model-based analysis of ChIP-Seq (MACS) (Zhang et al. 2008) under the threshold of q-value ≤ 0.05 revealed 14,211 peaks for ZmNAC128 and 9,261 peaks for ZmNAC130 (Supplemental Data Set 2), of which 7,082 peaks were common between the 2 NACs. We determined that approximately 60% of all the peaks bound by the 2 NACs were in the genic region approximately 3 kb from the transcription start site (TSS), of which more than 40% (4,811 genes) were within 1 kb of the TSS (Fig. 2C). Further analysis showed that the peaks were strongly concentrated immediately upstream of the TSS (Fig. 2D), consistent with the function of ZmNAC128 and ZmNAC130 as TFs.

To identify putative target genes of ZmNAC128 and ZmNAC130, these 4,811 genes with NAC-binding peaks

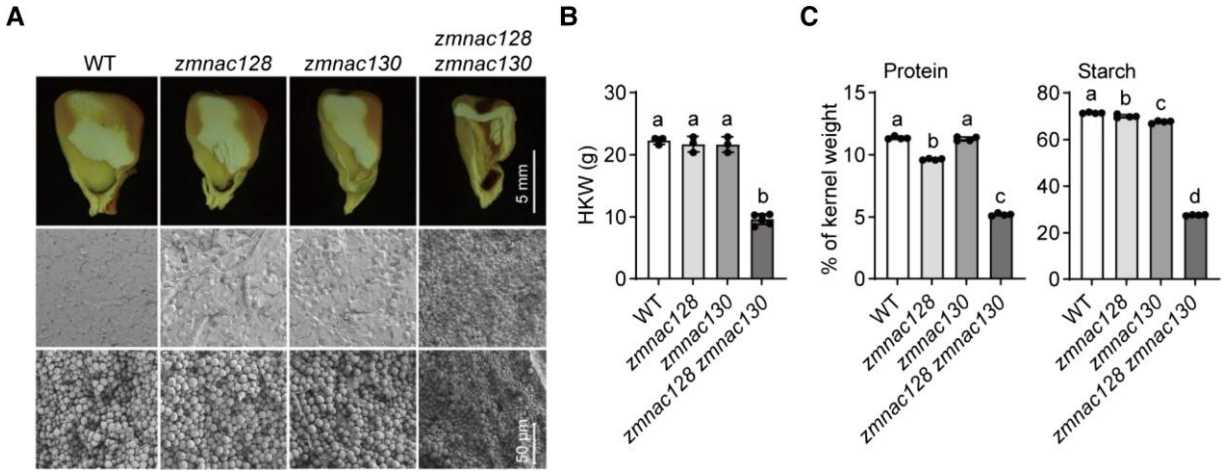

Figure 1. Knockout mutation of *ZmNAC128* and *ZmNAC130* causes poorly filled kernel phenotypes. **A)** Kernel phenotype of KN5585 (wild type, WT), *zmnac128*, *zmnac130*, and *zmnac128 zmnac130*. Top, mature kernel longitudinal sections; middle and bottom, scanning electron microscope of kernel longitudinal sections shown above. Middle, kernel peripheral region; bottom, kernel inner region. **B)** The HKW of mature kernels of the 3 mutants compared to the WT. g, gram. **C)** NIR analysis was conducted to determine the percentage of protein and starch accounting for kernel weight. The calibration of the NIR model utilized mature kernel flours from various maize varieties, as explained in detail in the "Materials and Methods" section. The protein or starch content in each kernel is expressed as a percentage (%) of kernel weight, calculated by comparing NIR-derived value to kernel weight. Data represent means ± standard deviation (SD) of at least 3 independent samples for each genotype **(B** and **C)**. Different lowercase letters indicate significant differences according to a one-way ANOVA with Tukey's multiple comparisons test ($P < 0.05$).

around 1 kb of TSS were overlapped with DEGs of *zmnac128 zmnac130* versus the WT in the KN5585 genetic background. Venn diagram results showed that 248 upregulated and 250 downregulated genes overlapped as putative direct targets (Supplemental Fig. S2 and Supplemental Data Set 3). These identified genes were further compared with DEGs of *zmnac128 zmnac130* in the KN5585 × B73 background of this study, of which 138 downregulated and 64 upregulated genes were common to both genetic backgrounds (Supplemental Data Set 4). They included multiple plant hormone-related genes, TFs, putative transporters, sugar metabolism genes, and so on. Among them, the 2 amino acid metabolism genes, *proline oxidase* (Zm00001eb022980) and *lysine-ketoglutarate reductase/saccharopine dehydrogenase 1* (*LKR/SDH1*, Zm00001eb192910), are not only the potential targets of ZmNAC128 and ZmNAC130 but also the direct targets of O2 (Li et al. 2015; Zhan et al. 2018).

ZmNAC128 and ZmNAC130 bind to the promoters of 16-kD γ-zein and Bt2

16-kD γ-zein and *Bt2* were previously identified as direct target genes of the 2 NACs (Zhang et al. 2019). Visualization of the DAP-seq data by the integrated genomics viewer (IGV) showed that the identified cis-element ACGCAA was surrounded by binding peaks for ZmNAC128 and ZmNAC130 in the promoters of *16-kD γ-zein* and *Bt2* (Fig. 2E). This suggested that our DAP-seq data are robust for the detection of potential target genes. We thus explored the genome-wide cis-elements bound by the 2 NACs via the motif discovery tool MEME-ChIP. The most significant cis-element bound by ZmNAC128 and ZmNAC130 was ACGCAA (E-value < 5.7E−149) (Fig. 2F), which was identical to the previously identified cis-element in the promoters of *16-kD γ-zein* and *Bt2* (Zhang et al. 2019). In addition to this motif, multiple candidate binding motifs were detected by DAP-seq (Supplemental Fig. S3). These candidates were highly identical either in the 2 independent replicates or between ZmNAC128 and ZmNAC130, suggesting that the 2 NACs also recognize other cis-elements in addition to the ACGCAA motif. Although multiple enriched elements are commonly detected in the DAP-seq analysis of ZmNAC128 and ZmNAC130, some of them could be binding motifs for their cofactors. For instance, the core motif "ACGT" recognized by bZIP-type TFs (such as O2) is also enriched in the DAP-seq of ZmNAC128 and ZmNAC130, but it requires additional investigation.

27-kD and 50-kD γ-zein are direct targets of ZmNAC128 and ZmNAC130

Consistent with the downregulated expression of all zein family genes in *zmnac128 zmnac130* (Supplemental Table S1), overall zein protein abundance was also lower in mature kernels of *zmnac128 zmnac130*, with the 16-kD γ-zein protein being nearly undetectable (Supplemental Fig. S4). These results thus supported the notion that, in addition to O2, ZmNAC128, and ZmNAC130 are also core TFs involved in zein gene expression. To investigate the regulation of ZmNAC128 and ZmNAC130 on the expression of other zein genes, we examined the DAP-seq data in detail. We observed peaks corresponding to the binding of ZmNAC128 and ZmNAC130 in the promoters of the other 2 γ-zein genes, *27-kD* and *50-kD γ-zein* (Fig. 3A). We detected the conserved motif ACGCAA around the binding peak regions in the promoters at −1,421/−1,464 and −461 bp upstream from the start codon of *27-* and *50-kD γ-zein* genes, respectively (Fig. 3A).

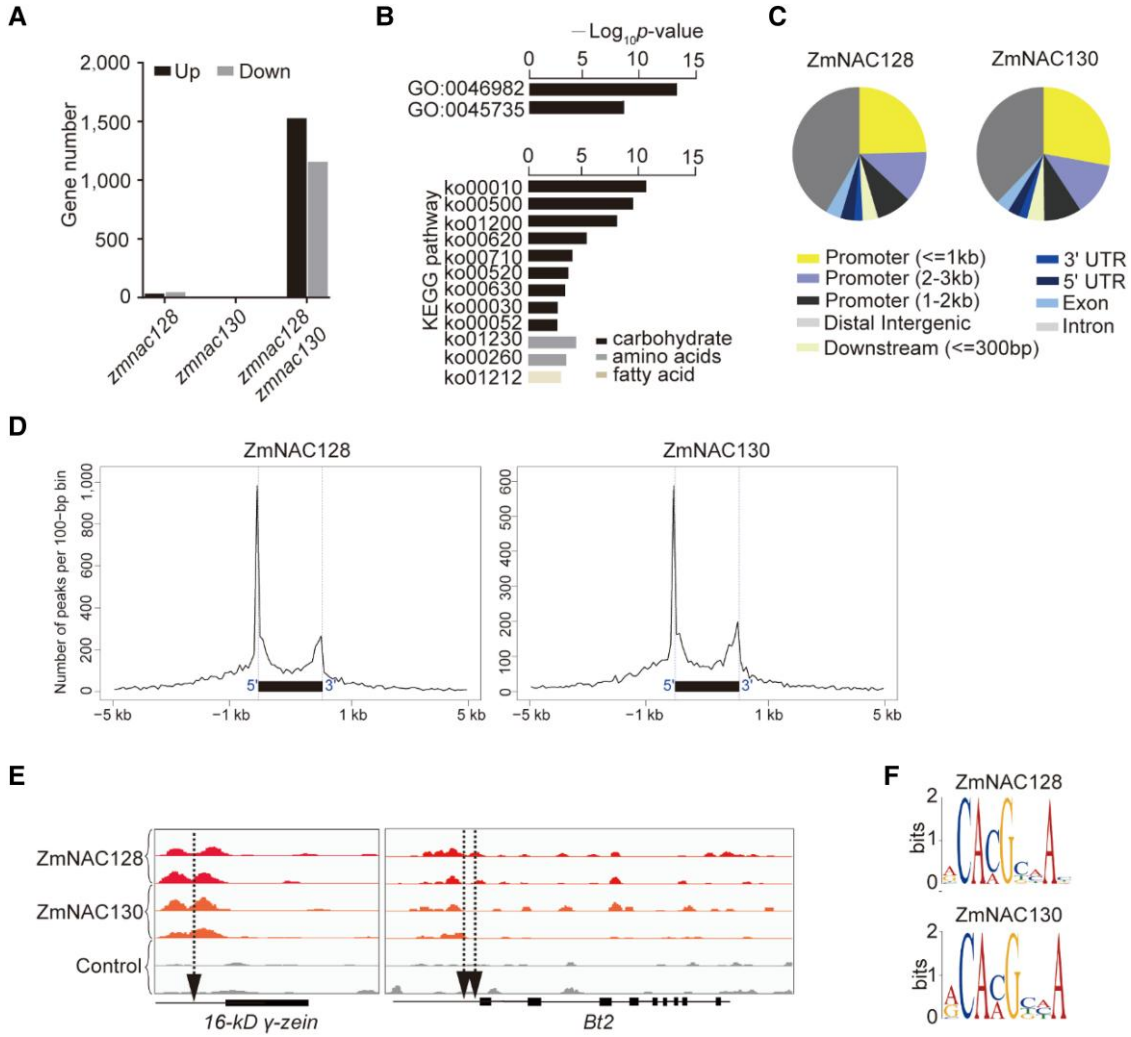

Figure 2. RNA-seq combined with DAP-seq investigating the direct targets of ZmNAC128 and ZmNAC130. **A)** Number of upregulated and downregulated expressed genes in *zmnac128*, *zmnac130*, and *zmnac128 zmnac130*, compared to the WT. DEGs were identified based on FC ≥2 and *P*-value ≤0.05. **B)** Significantly enriched GO terms and KEGG pathways based on DEGs of *zmnac128 zmnac130*. GO:0046982 (protein heterodimerization activity); GO:0045735 (nutrient reservoir activity); ko00010 (glycolysis/gluconeogenesis); ko00500 (starch and sucrose metabolism); ko01200 (carbon metabolism); ko00620 (pyruvate metabolism); ko00710 (carbon fixation in photosynthetic organisms); ko00520 (amino sugar and nucleotide sugar metabolism); ko00630 (glyoxylate and dicarboxylate metabolism); ko00030 (pentose phosphate pathway); ko00052 (galactose metabolism); ko01230 (biosynthesis of amino acids); ko00260 (glycine, serine and threonine metabolism); ko01212 (fatty acid metabolism). **C)** Distribution of ZmNAC128 and ZmNAC130 binding regions in the maize genome. **D)** Metaplots showing the distribution of ZmNAC128 and ZmNAC130 binding peaks per 100-bp bin corresponding to the −1,000- to +2,000-bp region flanking the transcription start site (TSS). **E)** IGV shows the distribution of ZmNAC128- and ZmNAC130-binding peaks in the promoters of *16-kD γ-zein* and *Bt2*. For ZmNAC128, ZmNAC130, and IgG (control), 2 independent experiments were performed. Aligned reads are indicated in red (ZmNAC128), orange (ZmNAC130), or gray (IgG). The y-axis (or peaks) represents the number (or accumulation) of the aligned reads. The relative positions of the element ACGCAA are marked by arrowheads. **F)** The most significant elements of ZmNAC128 and ZmNAC130 according to MEME-ChIP analysis.

To test the binding of ZmNAC128 and ZmNAC130 to the fragments containing ACGCAA in the 2 promoters, we performed the ChIP-qPCR assay. For this assay, we used an antibody against the Flag tag and the 16-DAP endosperms of the transgenic lines of 3×Flag-tagged ZmNAC128 and ZmNAC130 that are driven by the *27-kD γ-zein* promoter (Supplemental Fig. S5). The ChIP-qPCR results verified the binding relationship of ZmNAC128 and ZmNAC130 in the 2 γ-zein gene promoters revealed by our DAP-seq analysis (Fig. 3B). A dual-luciferase reporter (DLR) assay was thus performed to assess the transactivation activities of ZmNAC128 and ZmNAC130 for the expression of firefly luciferase (LUC)-encoding gene driven by the 2 promoters in maize leaf protoplast cells. Compared to the empty vector control, LUC activities driven by the *27-kD γ-zein* promoter could be significantly increased by the cotransformation of 35S promoter-driven *ZmNAC128* or *ZmNAC130*. Similarly, LUC activities driven by the *50-kD γ-zein* promoter were also significantly increased by ZmNAC128 or ZmNAC130 (Fig. 3C). Similar to

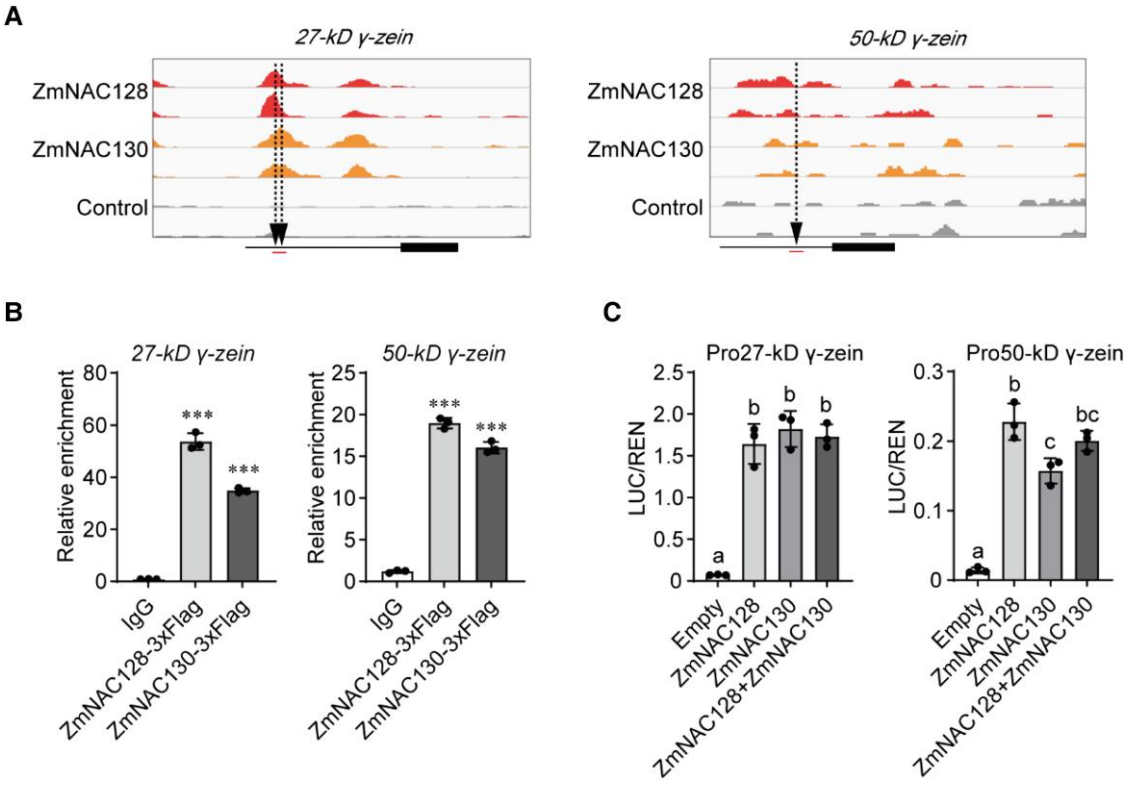

Figure 3. Verification of *27-kD γ-zein* and *50-kD γ-zein* as the direct targets of ZmNAC128 and ZmNAC130. **A)** IGV shows the peaks bound by ZmNAC128 and ZmNAC130 in these 2 promoters. The relative positions of the element ACGCAA are marked by arrowheads. **B)** ChIP-qPCR detects the in vivo binding activities of ZmNAC128 and ZmNAC130 to these 2 promoters. The red lines under the arrowheads in **(A)** indicate the region detected by ChIP-qPCR. ChIP products of IgG were used as a negative control. *ACTIN* was used as an internal control. **C)** DLR detects the transactivation activities of ZmNAC128 and ZmNAC130 on the 2 promoters. The results were also shown in Supplemental Fig. S17. Data represent means ± SD of 3 independent samples for each test **(B** and **C)**. Significance differences (***$P < 0.001$) were determined by a Student's *t*-test **(B)**. Different lowercase letters indicate significant differences according to a one-way ANOVA with Tukey's multiple comparisons test ($P < 0.05$) **(C)**.

the *16-kD γ-zein* promoter (Zhang et al. 2019), LUC activities driven by the 2 promoters were not stronger under the coexpression of both ZmNAC128 and ZmNAC130 (Fig. 3C).

Combining these results with our previous findings (Zhang et al. 2019), we concluded that ZmNAC128 and ZmNAC130 are direct transcriptional regulators of all 3 (*50-*, *27-*, and *16-kD*) *γ-zein* genes. We previously found that the PB number is significantly reduced in the filling endosperm of *nacRNAi* lines (Zhang et al. 2019). As γ-zein proteins are essential for PB formation, ZmNAC128 and ZmNAC130 are likely to play important roles in PB formation. There were no apparent DAP-seq peaks in other zein gene promoters, so the expression of other zein genes is possibly regulated by their cofactors.

ZmNAC128 and ZmNAC130 directly regulate the expression of multiple important starch metabolism genes

Reduced starch content and enrichment of the starch and sucrose metabolism KEGG pathways among the observed DEGs of *zmnac128 zmnac130* suggest that the 2 NACs may directly regulate the expression of genes involved in starch metabolism. We previously found that the expression of multiple important starch metabolism genes was downregulated in the *nacRNAi*, but only *Bt2* was characterized as the direct target gene of ZmNAC128 and ZmNAC130 (Zhang et al. 2019).

To study which starch metabolism genes are the direct targets of ZmNAC128 and ZmNAC130, we emphasized the commonly downregulated genes in the 16-DAP endosperms of both *zmnac128 zmnac130* and *nacRNAi* (Table 1). In all 7 downregulated genes in the *nacRNAi* (Zhang et al. 2019), 6 genes were also detected to be significantly downregulated in *zmnac128 zmnac130*, including *Bt2* (Zm00001eb176800), *pullulanase-type starch debranching enzyme* (*Zpu1*, Zm00001eb088740), *SS1* (Zm00001eb376100), *Sus1* (Zm00001eb392880), *granule-bound starch synthase 1* (*GBSS1*, also named *waxy* [*Wx*], Zm00001eb378140), *starch branching enzyme IIb* (*SBEIIb*, also named *amylose extender1* [*Ae1*], Zm00001eb242610) (Supplemental Data Set 5). *Starch branching enzyme 1* (*SBE1*, Zm00001eb228530) was detected to be transcriptionally downregulated only in the *nacRNAi* (Zhang et al. 2019), but its encoded protein was not reduced in *zmnac128 zmnac130* compared to the WT (Fig. 4A).

Meanwhile, transcriptome analysis of *zmnac128 zmnac130* found that another 2 important starch metabolism genes also significantly downregulated, including *isoamylase-type starch-*

Table 1. Summary of promoter analysis of starch metabolism genes and their expression in *nacRNAi* and *zmnac128 zmnac130*

Gene name	Binding peaks	Cis-element ACGCAA	*nacRNAi*		*zmnac128 zmnac130*	
			mRNA	Protein	mRNA	Protein
Bt2	Y	Y	Down.	Reduced	Down.	Reduced
Zpu1	Y	Y	Down.	n.d.	Down.	Reduced
GBSS1	Y	Y	Down.	n.d.	Down.	Reduced
SS1	Y	Y	Down.	n.d.	Down.	Reduced
Sus1	Y	Y	Down.	n.d.	Down.	n.d.
SBEIIb	Y	N	Down.	n.d.	Down.	Reduced
SSIIa	Y	Y	n.s.	n.d.	Down.	Reduced
ISA1	N	N	n.s.	n.d.	Down.	Reduced
Sh2	N	Y	n.s.	n.d.	n.s.	Reduced
Sh1	N	Y	n.s.	n.d.	n.s.	Reduced
SSIII	N	Y	n.s.	n.d.	n.s.	Reduced
SSV	N	Y	n.s.	n.d.	n.s.	Reduced
Bt1	Y	N	n.d.	n.d.	n.s.	Reduced
SBE1	N	N	Down.	n.d.	n.s.	n.s.

Note: The data of *nacRNAi* from Zhang et al. (2019). The data of *zmnac128 zmnac130* from this study. Y, Yes; N, No; down., downregulated; n.d., no detection; n.s., not significantly downregulated or reduced.

debranching enzyme1 (*ISA1*, also named *sugary1* [*Su1*], Zm00001eb242610) and *starch synthase IIa* (*SSIIa*, also named *sugary2* [*Su2*], Zm00001eb279740) (Supplemental Data Set 5). Therefore, the complete elimination of *ZmNAC128* and *ZmNAC130* through CRISPR/Cas9-mediated knockout caused the downregulated expression of more important starch metabolism genes than their RNAi-mediated knockdown.

To detect the effects of ZmNAC128 and ZmNAC130 on starch metabolism, we performed a suite of immunoblotting assays with antibodies against the major starch metabolism enzyme proteins in 20-DAP endosperms of *zmnac128 zmnac130* and the WT (Fig. 4A). Consistent with the pronounced reduction in *Zpu1* and *Bt2* transcripts, their corresponding protein accumulation also decreased by nearly 80% in *zmnac128 zmnac130* compared to the WT. Moreover, the accumulation of 4 starch biosynthesis enzymes, including GBSS1, SS1, SSIIa, and ISA1 decreased by more than 50% in *zmnac128 zmnac130* compared to the WT. The accumulation of multiple other enzymes (AGPase large subunit shrunken2 [Sh2], Sh1, SBEIIb, SSIII, SSV, and ADP-glucose transporter brittle endosperm 1 [Bt1]) decreased by 20% to 50% in *zmnac128 zmnac130* compared to the WT. Taken together, these results indicated that almost all the detected proteins accumulated to lower levels in *zmnac128 zmnac130* than in the WT. This could be one main cause for the dramatic reduction in starch content and kernel weight of *zmnac128 zmnac130*.

To investigate which genes were directly regulated by ZmNAC128 and ZmNAC130, we did the DAP-seq and promoter analysis. In these 8 downregulated starch metabolism genes in *zmnac128 zmnac130*, 7 genes (*Bt2*, *Zpu1*, *GBSS1*, *SS1*, *SSIIa*, *Sus1*, and *SBEIIb*) were found to have binding peaks of ZmNAC128 and ZmNAC130 in their promoters (Table 1). Besides *Bt2* (Fig. 2E), the promoters of another 5 genes (*Zpu1*, *GBSS1*, *SS1*, *SSIIa*, and *Sus1*) also contained the conserved cis-element ACGCAA at positions −1, −394/−692, −2,664, −875/−970, and −1,613/−1,627 upstream from their corresponding TSS, respectively (Fig. 4B). Sh1, Sh2, SSIII, SSV, and Bt1 exhibited reduced protein accumulation without a corresponding decrease in transcript level. Notably, although the promoters of 4 of these genes (*Sh1*, *Sh2*, *SSIII*, and *SSV*) contain the element ACGCAA, no binding peaks were detected in any of the 4 promoters (Table 1 and Supplemental Fig. S6).

In contrast, despite the absence of the conserved cis-element ACGCAA in the promoters of *Bt1* and *SBEIIb*, binding peaks were still detected in both promoters (Table 1), indicating that NACs can bind to these promoters even in the absence of their canonical target sequence. ChIP-qPCR further verified the binding relationships of ZmNAC128 and ZmNAC130 for these 5 promoters of *Zpu1*, *GBSS1*, *SS1*, *SSIIa*, and *Sus1* (Fig. 4C). Finally, DLR assays were performed to detect the transactivation activities of ZmNAC128 and ZmNAC130 with respect to the 5 promoters. LUC activities driven by the 4 promoters of *Zpu1*, *GBSS1*, *SS1*, and *SSIIa* were significantly increased by the co-transformation of 35S promoter-driven ZmNAC128 and ZmNAC130 (Fig. 4D). The *Sus1* promoter was slightly transactivated only by ZmNAC130 but not ZmNAC128. This suggested that although ZmNAC128 and ZmNAC130 can bind to this promoter, its transactivation potentially requires the involvement of other TFs. Similarly, the LUC activities driven by these 5 promoters were not stronger upon co-expression of ZmNAC128 and ZmNAC130. Because both the transcript levels and protein accumulation of *Bt2*, *Zpu1*, *GBSS1*, *SS1*, and *SSIIa* were significantly reduced in *zmnac128 zmnac130*, ZmNAC128 and ZmNAC130 function as core TFs for starch metabolism through the direct regulation of these starch metabolism genes, i.e. *Bt2*, *Zpu1*, *GBSS1*, *SS1*, *SSIIa*, and *Sus1*.

Because carbohydrate-related pathways were generally enriched in DEGs in *zmnac128 zmnac130*, we also analyzed the expression of genes involved in the 3 primary carbohydrate

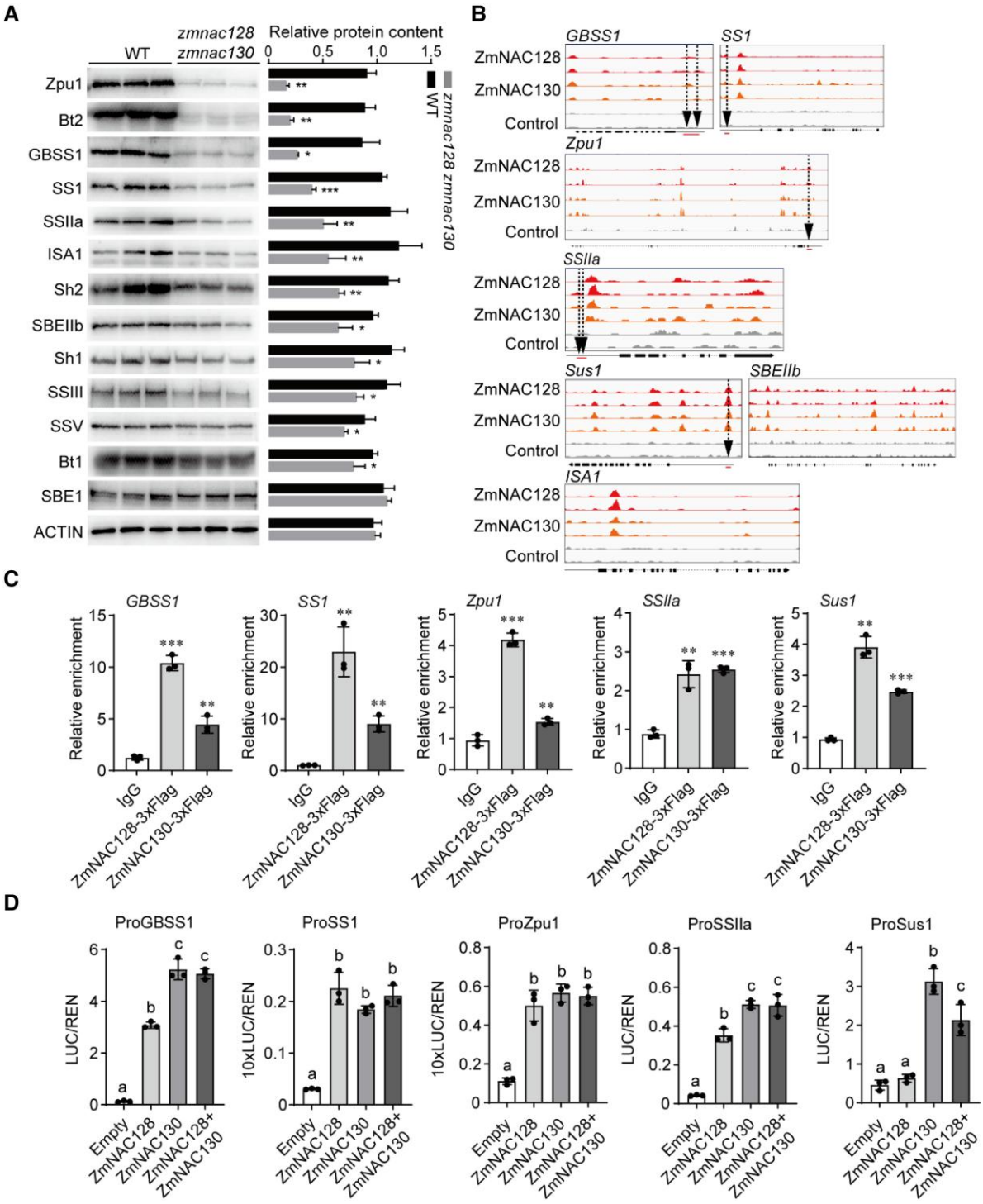

Figure 4. Verification of starch metabolism genes as direct targets of ZmNAC128 and ZmNAC130. **A)** Immunoblotting of protein accumulation for the major starch metabolism enzymes in 20-DAP endosperms of *zmnac128 zmnac130* and WT. The 20 ng nonzein proteins per lane were loaded, while ACTIN served as the loading control. The original and intact images were shown in Supplemental Fig. S21. Three independent samples for each material were performed and quantified by the ImageJ software. For each starch metabolism enzyme, protein abundance in *zmnac128 zmnac130* was normalized to the corresponding WT, which was set to 1. **B)** IGV shows binding peaks in the promoters of genes transcriptionally downregulated in *zmnac128 zmnac130*. The relative positions of the cis-element ACGCAA are marked by arrowheads. **C)** ChIP-qPCR detects the in vivo binding activities of ZmNAC128 and ZmNAC130 to the 5 promoters. The red lines under the arrowheads in **(B)** indicate the region detected by ChIP-qPCR. **D)** DLR detects the transactivation activities of ZmNAC128 and ZmNAC130 on these 5 promoters. Data represent means ± SD of 3 independent samples for each test **(A**, **C**, and **D)**. Significance differences (**$P < 0.01$ and ***$P < 0.001$) were determined by a Student's *t*-test **(A** and **C)**. Different lowercase letters indicate significant differences according to a one-way ANOVA with Tukey's multiple comparisons test ($P < 0.05$) **(D)**.

metabolism pathways: the pentose phosphate pathway, glycolysis, and the tricarboxylic acid cycle. In contrast to the overall downregulated expression of starch metabolism genes, many genes in these 3 pathways were upregulated in *zmnac128 zmnac130* (Supplemental Data Set 5). The upregulated expression of many genes involved in these 3 primary carbohydrate metabolism pathways seems to indicate negative feedback due to a sharp decrease in starch metabolism in the endosperm of *zmnac128 zmnac130*, but this hypothesis needs to be investigated.

Regulatory and physical interactions of ZmNAC128 and ZmNAC130 with O2

Among known endosperm filling-related TF genes, *O2*, *ZmNAC128*, and *ZmNAC130* are the most highly expressed in the filling-stage endosperm (Chen et al. 2014). Based on the 3 RNA-seq datasets from the *ZmNAC128* and *ZmNAC130* knockdown lines and knockout mutants in this study and our previous publication (Zhang et al. 2019), we observed that the expression of the *O2* gene is consistently downregulated in *nacRNAi* and *zmnac128 zmnac130* compared to the corresponding NT and WT, respectively (Supplemental Fig. S7). Importantly, only a few DEGs were shared across studies, one of which was *O2*, making this TF a candidate target gene of ZmNAC128 and ZmNAC130.

ZmNAC128 and ZmNAC130 directly regulate the expression of O2

To test whether the 2 NACs regulate the expression of *O2*, we further measured the transcript level and protein accumulation of *O2* in the endosperms of *zmnac128 zmnac130* across the entire filling stages from 12- to 28-DAP. RT-qPCR analysis showed that the transcript levels of *O2* decreased by nearly 50% on average in the endosperm of *zmnac128 zmnac130* throughout the whole filling stage (Fig. 5A). Likewise, the protein accumulation of O2 significantly decreased by 60% to 80% in endosperms of *zmnac128 zmnac130* throughout the whole filling stage (Fig. 5B and Supplemental Fig. S8). These findings support a role for ZmNAC128 and ZmNAC130 in maintaining the high expression of *O2* in the endosperm across the whole filling stage.

To know whether ZmNAC128 and ZmNAC130 directly regulate the expression of *O2*, we first examined the DAP-seq data. There were apparent peaks corresponding to regions bound by ZmNAC128 and ZmNAC130 in the *O2* promoter (Fig. 5C). The peak encompassing binding region contains the maize ABSCISIC ACID INSENSITIVE3 transcription factor 19 (ZmABI19)-binding RY motif (CATGCATG), the O2/O11-binding core motif (ACGT), and 3 candidate ZmNAC128/130-binding motifs (GTACGT, CTAGCTA, and TTGCTT) (Fig. 5C). To ascertain which candidate motif in the *O2* promoter can be recognized by ZmNAC128 and ZmNAC130, we conducted an electrophoretic mobility shift assay (EMSA) involving recombinant His-ZmNAC128 and His-ZmNAC130 and 5 biotin-labeled probes covering a 151-bp region from −510 to −360 bp upstream from the start codon of *O2* gene (Fig. 5D). Only the P3 fragment was bound by ZmNAC128 and ZmNAC130, to form retarded bands in the gel, and ChIP-qPCR also confirmed this binding relationship (Fig. 5E). The binding specificity of ZmNAC128 and ZmNAC130 was furthermore verified through the addition of 50× and 200× unlabeled P3 probes in the reactions, which caused a progressive loss of retarded bands (Supplemental Fig. S9).

Subsequently, GTACGT in the P3 was subjected to point mutation analysis. Any point mutation could abolish the binding interaction of ZmNAC128 and ZmNAC130, confirming GTACGT as an additional cis-element (Fig. 5D). Finally, a DLR assay was conducted to determine the transactivation ability of ZmNAC128 and ZmNAC130 with respect to the *O2* promoter. Compared to the empty vector control, LUC activities driven by the *O2* promoter were significantly increased by ZmNAC128 or ZmNAC130, and the co-expression of the 2 NACs resulted in slightly but significantly stronger transactivation compared to each individual NAC alone (Fig. 5F). These results indicated that these 2 NACs play crucial roles in directly activating the high expression of *O2*.

Physical interactions of these 3 TFs

To test the physical interaction between the 3 TFs, we performed a series of in vitro and in vivo protein–protein interaction assays pull-down, bimolecular fluorescence complementation (BiFC), LUC complementation imaging (LCI), and co-immunoprecipitation (Co-IP) assays. The pull-down assay results showed that glutathione S-transferase (GST)-tagged O2 interacts with His-tagged ZmNAC128 but not ZmNAC130, while GST-tagged ZmNAC130 interacts with His-tagged ZmNAC128 (Fig. 6A, Supplemental Fig. S10). For BiFC and LCI assays, we cloned the coding sequences of each TF-encoding gene in-frame with the sequence encoding the N-terminal or C-terminal half of yellow fluorescent protein (YFP) or LUC, after which we transformed the resulting constructs into Agrobacterium (*Agrobacterium tumefaciens*) strain GV3101.

Unlike for the negative control with no visible signals, we detected YFP signals and LUC activity in the *Nicotiana benthamiana* leaves co-infiltrated with *ZmNAC128* and *O2* constructs as well as in those co-infiltrated with the *ZmNAC128* and *ZmNAC130* constructs (Fig. 6B, Supplemental Figs. S10 and S11). We also conducted a Co-IP assay in which we cloned *ZmNAC128* and *ZmNAC130* in-frame with a sequence encoding 6×Myc, while *O2* and *ZmNAC130* were cloned in-frame with a 3×Flag sequence, after which each construct was transiently co-infiltrated in *N. benthamiana* leaves. We detected a band of the expected molecular

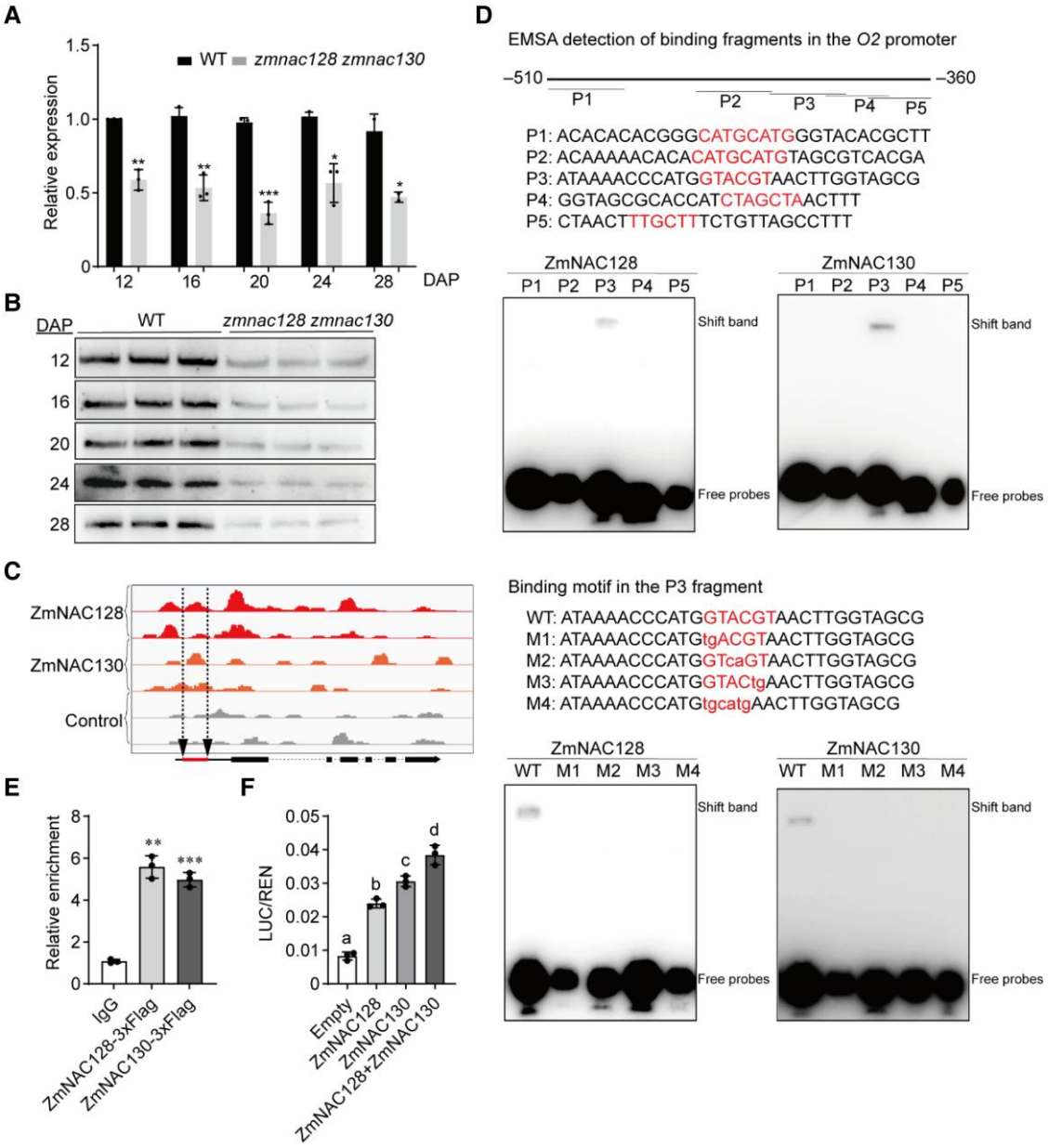

Figure 5. ZmNAC128 and ZmNAC130 regulate the expression of *O2* in the filling endosperm. **A)** RT-qPCR of *O2* expression in the filling endosperms of *zmnac128 zmnac130* and WT. Relative expression was normalized to *ACTIN*. Data represent means ± SD of 3 independent samples for each time point except for 2 samples at 28 DAP. Statistical significance was determined by a Student's *t*-test. $^{*}P < 0.05$, $^{**}P < 0.01$, $^{***}P < 0.001$. **B)** Immunoblotting of O2 protein in the filling endosperms of *zmnac128 zmnac130* and WT. The 20 ng nonzein proteins per lane were loaded. The quantification was shown in Supplemental Fig. S8. **C)** IGV shows the peaks bound by ZmNAC128 and ZmNAC130 in the *O2* promoter. The relative region covering 4 candidate elements, CATGCATG, GTACGT, CTAGCTA, and TTGCTT, are marked by a red line in the promoter. **D)** EMSA detects an additional cis-element of ZmNAC128 and ZmNAC130 in the *O2* promoter. Upside: 5 biotin-labeled probes in the region of −510 to −360 upstream from the start codon are listed, and the 5 probes contained the above-mentioned 4 candidate elements. Underside: the 6-bp GTACGT box in the P3 probe (WT) and 3 mutant probes were produced by 2-bp mutations in the 6-bp box. **E)** ChIP-qPCR detects the in vivo binding activity of ZmNAC128 and ZmNAC130 to the *O2* promoter. A red line in the *O2* promoter in **(C)** indicates the region detected by ChIP-qPCR. **F)** DLR detects the transactivation activities of ZmNAC128 and ZmNAC130 on the *O2* promoter. Data represent means ± SD of 3 independent samples for each test **(E** and **F)**. Significance differences ($^{**}P < 0.01$ and $^{***}P < 0.001$) were determined by a Student's *t*-test **(E)**. Different lowercase letters indicate significant differences according to a one-way ANOVA with Tukey's multiple comparisons test ($P < 0.05$) **(F)**.

weight for Myc-ZmNAC128 in the protein extracts immunoprecipitated with anti-Flag antibodies from leaves co-expressing *Flag-O2* (or *Flag-ZmNAC130*) and *Myc-ZmNAC128* (Fig. 6C). These results demonstrated that ZmNAC128 interacts with O2, ZmNAC130, and itself, while ZmNAC130 interacts with ZmNAC128 and itself.

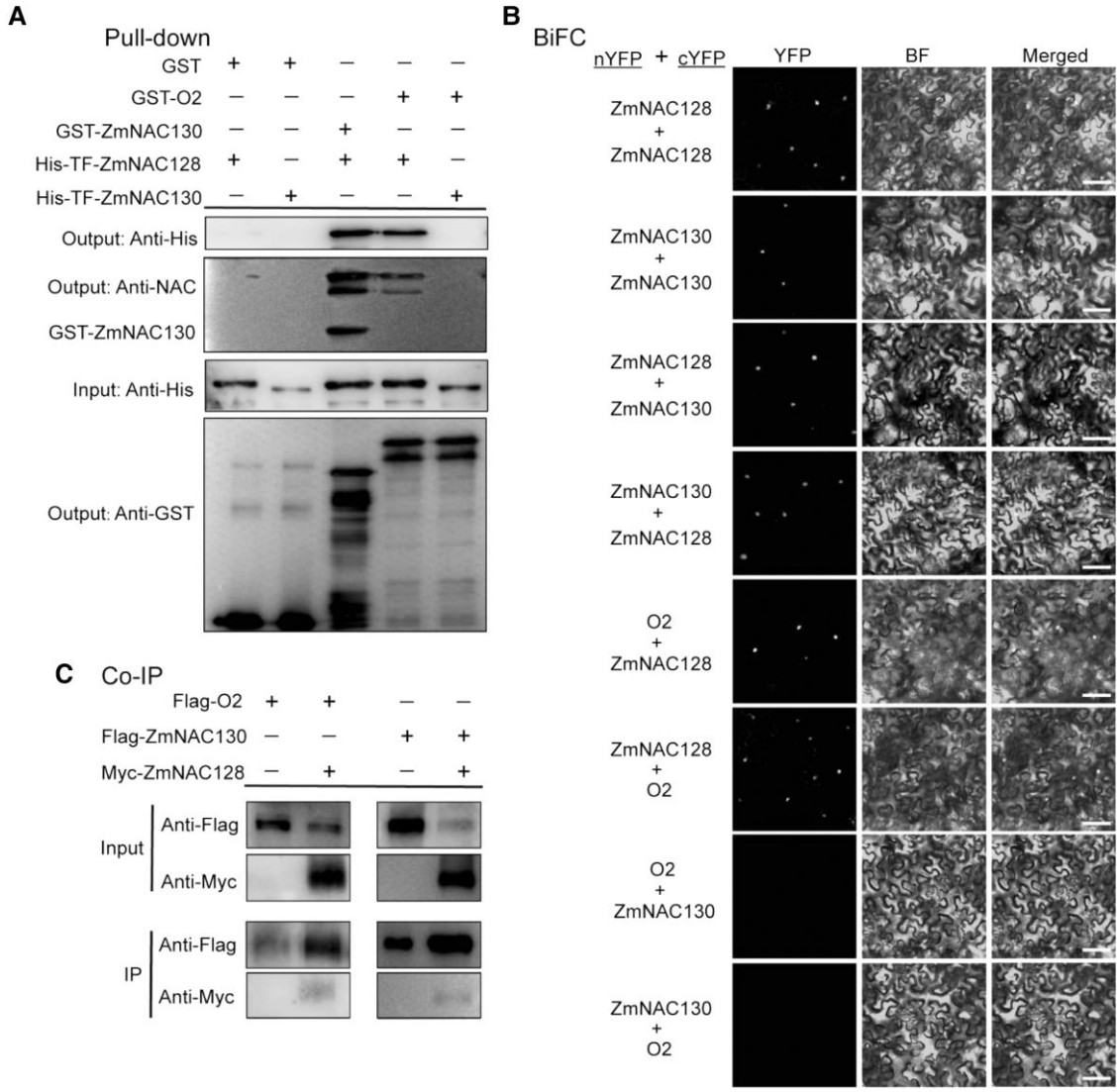

Figure 6. In vitro and in vivo protein interaction assays show the physical interaction of O2, ZmNAC128, and ZmNAC130. **A)** GST pull-down detects the interactions between recombinant purified proteins of O2, ZmNAC128, and ZmNAC130. **B)** BiFC detects the interactions between O2, ZmNAC128, and ZmNAC130. Negative controls in Supplemental Fig. S11. BF, bright field. Scale bars, 50 μm. **C)** Co-IP detects the interactions between O2, ZmNAC128, and ZmNAC130. The indicated plasmids (harboring Flag or Myc tags) were transformed and subsequently co-expressed in *N. benthamiana* leaves. The Flag-fused proteins were immunoprecipitated, and the precipitates were probed with anti-Flag or anti-Myc antibodies.

Combined effects of ZmNAC128, ZmNAC130, and O2 on the regulation of endosperm filling

To investigate the combined effects of the 3 TFs on the endosperm filling, we generated a triple mutant *zmnac128 zmnac130 o2*. The 2 loss-of-function mutants of *O2* were identified by screening an ethyl methanesulfonate (EMS)-mutagenized B73 library and were backcrossed to B73 for several generations. We named the 2 mutant alleles *o2-1*, which has a premature stop codon in the first exon, and *o2-2*, which has an acceptor splice site mutation between the first intron and the second exon (Supplemental Fig. S12). In this study, *o2-1* was used for crossing with *zmnac128 zmnac130*.

We isolated homozygous mutants for *zmnac128 zmnac130*, *o2*, and *zmnac128 zmnac130 o2* from the offspring of the same F_2 cob resulting from the *zmnac128 zmnac130* × *o2* cross. The triple mutant *zmnac128 zmnac130 o2* exhibited a more poorly filled kernel phenotype than did *zmnac128 zmnac130* (Fig. 7A). Compared to that of the NT segregated from *zmnac128 zmnac130* × *o2* cross, the HKWs of *o2*, *zmnac128 zmnac130*, and *zmnac128 zmnac130 o2* decreased by 26%, 55%, and 73%, respectively (Fig. 7B). Compared to the NT, the mature kernels of *zmnac128 zmnac130 o2* exhibited an 80% decrease in starch content and a 50% decrease in protein content (Fig. 7C).

We further performed RNA-seq analysis of 16-DAP endosperms from *o2*, *zmnac128 zmnac130*, *zmnac128 zmnac130 o2*, and the NT. Principal component analysis showed that the transcriptome of *zmnac128 zmnac130 o2* is more similar

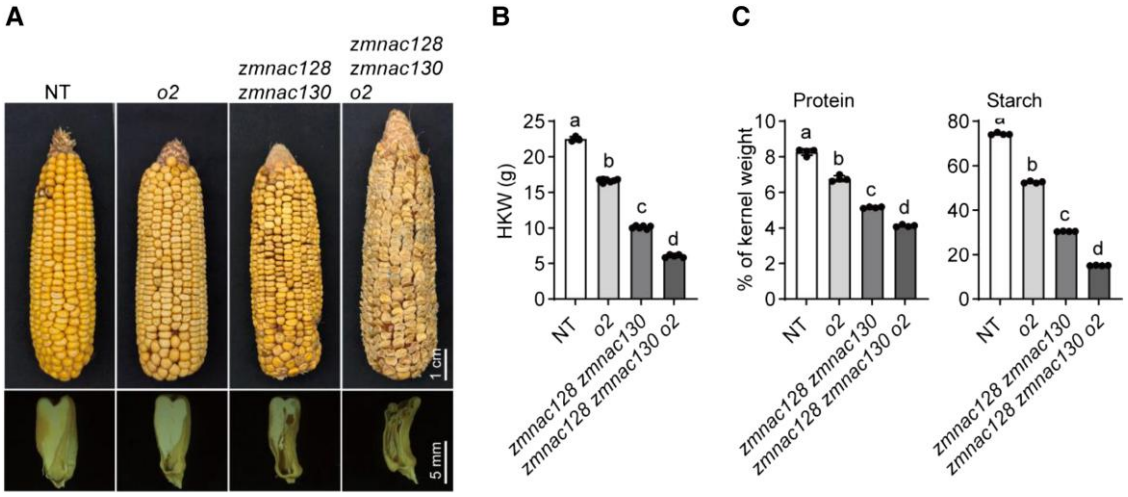

Figure 7. The triple mutation of *O2*, *ZmNAC128*, and *ZmNAC130* causes a more poorly filled kernel phenotype. **A)** Mature cobs and kernel longitudinal sections of *o2*, *zmnac128 zmnac130*, and *zmnac128 zmnac130 o2* compared to the NT in the KN5585 × B73 background. **B)** The HKW analysis of the 4 genetic materials. **C)** Determination of protein and starch in the mature kernels from the 4 genetic materials. Data represent means ± SD of at least 3 independent samples for each genotype (**B** and **C**). Different lowercase letters indicate significant differences according to a one-way ANOVA with Tukey's multiple comparisons test ($P < 0.05$) (**B** and **C**).

to that of *zmnac128 zmnac130* than *o2* (Fig. 8A). The number of DEGs was slightly higher in *zmnac128 zmnac130 o2* than in *zmnac128 zmnac130* but was twofold higher than in *o2* (Fig. 8B). A Venn diagram of the DEGs also illustrated that more than 60% of all the DEGs were shared between *zmnac128 zmnac130 o2* and *zmnac128 zmnac130*, while less than 30% of DEGs were shared between *zmnac128 zmnac130 o2* and *o2* (Fig. 8C). This suggested that the 2 NACs have stronger effects on endosperm filling than O2.

As these 3 TFs significantly impacted the transcriptome of filling-stage endosperms, it is likely that their shared downstream TFs play crucial roles in their GRN. We first detected their cotransactivation in their own promoters by a group of DLR assays. O2 was previously reported to exhibit autotransactivation (Lohmer et al. 1991; Yang et al. 2022a, 2022b). Our results demonstrated that the *O2* promoter exhibited a stronger transactivation effect in the presence of all 3 TFs than when they acted individually, indicating a synergistic effect of their co-expression (Supplemental Fig. S13). Transcriptome analysis indicated that *ZmNAC130* but not *ZmNAC128* is significantly downregulated in the *o2* mutant (Supplemental Fig. S14A). DLR results revealed that O2 can transactivate the promoter of *ZmNAC130*, but not that of *ZmNAC128*, which is consistent with their respective expression patterns in *o2* (Supplemental Fig. S14B).

Similar to the *O2* promoter, the promoters of *ZmNAC130* and *ZmNAC128* were found to be strongly activated by the co-expression of all 3 TFs (Supplemental Fig. S14B). In addition, several TFs have been reported as the direct downstream genes of O2, including *bZIP G-box binding factor 1* (*GBP1*), *MYBR13*, *bZIP17*, and *NKD2* (Li et al. 2015; Zhan et al. 2018). To detect which ones can also be the target genes of ZmNAC130 and ZmNAC128, we analyzed the binding peaks of ZmNAC128 and ZmNAC130 in these 4 gene promoters. Only the *MYBR13* promoter was apparently bound by both ZmNAC128 and ZmNAC130 (Supplemental Fig. S15A). DLR results indicated that all 3 TFs were capable of individually transactivating the *MYBR13* promoter, with the highest LUC activity observed in the co-expression of the 3 TFs (Supplemental Fig. S15B). Consistent with the promoter transactivation, the expression of *MYBR13* was the lowest in *zmnac128 zmnac130 o2* (Supplemental Fig. S15C), hinting at their synergistic regulation.

Combined effects of the three TFs on the regulation of zein synthesis

GO term enrichment analysis of the 581 DEGs common among the 3 mutants revealed that "nutrient reservoir activity" (GO: 0045735, *P*-value = 1.8E−18) was the most significantly enriched GO term (Supplemental Fig. S16). This is consistent with the strong influence of O2, ZmNAC128, and ZmNAC130 on the expression of zein family genes. The expression of all zein genes was lower in *zmnac128 zmnac130 o2* than in *zmnac128 zmnac130* or *o2* (Supplemental Data Set 6). Except for 27-kD γ-zein, most zein proteins were barely visible, as shown by Coomassie Brilliant Blue staining (Fig. 8D). In view of the transactivation of O2 on the promoters of *27-kD γ-zein* and *50-kD γ-zein*, our further detection indicated that ZmNAC128 and ZmNAC130 can coordinate with O2 to enhance the transactivation of the promoter of *50-kD γ-zein* but not that of *27-kD γ-zein* (Supplemental Fig. S17). Therefore, the synergistic effect of these 3 TFs on the expression of most zein genes seems similar to that of O2, PBF1, and OHPs, which do not involve direct transcriptional regulation (Zhang et al. 2015).

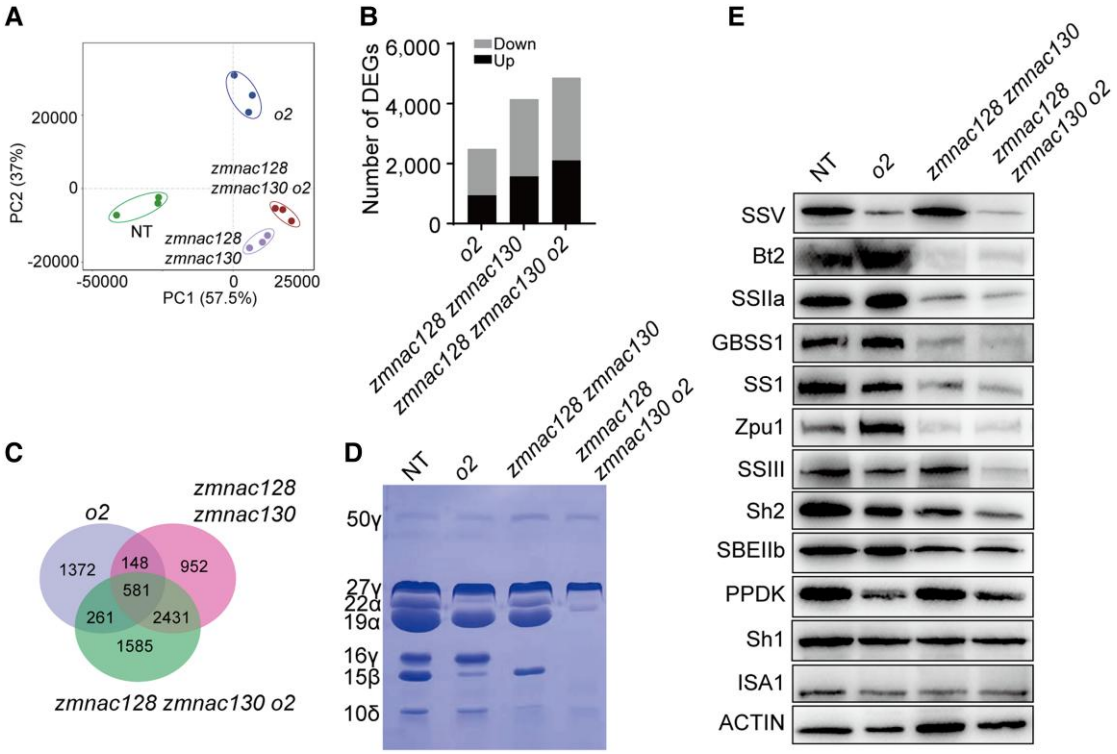

Figure 8. O2, ZmNAC128, and ZmNAC130 synergistically affect the expression of zeins and starch metabolism enzymes. **A)** Principal component analysis based on transcriptome data of the 4 genetic materials. There were 3 independent samples for each genotype. **B)** Number of DEGs in *o2*, *zmnac128 zmnac130*, and *zmnac128 zmnac130 o2* compared to the NT. DEGs were identified based on FC ≥ 2 and *P*-value ≤ 0.05. **C)** Venn diagram shows the overlap between these DEGs. **D)** Coomassie Brilliant Blue staining SDS-PAGE of zein proteins in mature kernels. The total zein proteins loaded in each lane are equal to 200 μg of mature kernel flour. Each band was indicated by the corresponding type of zein. 50γ, 50-kD γ-zein; 27γ, 27-kD γ-zein; 22α, 22-kD α-zein; 19α, 19-kD α-zein; 16γ, 16- kD γ-zein; 15β, 15-kD β-zein; 10δ, 10-kD δ-zein. **E)** Immunoblotting of protein accumulation of starch metabolism enzymes in the 20-DAP endosperm. The 20 ng nonzein proteins for each lane were loaded, while ACTIN was the loading control.

Combined effects of the three TFs on the regulation of starch synthesis

Consistent with the dramatic reduction in starch contents in mature *zmnac128 zmnac130 o2* kernels, starch accumulation decreased in the filling-stage endosperms of *zmnac128 zmnac130 o2* compared to *zmnac128 zmnac130* and *o2*, as evidenced by potassium iodide staining (Supplemental Fig. S18). However, the expression of most starch metabolism genes and other carbohydrate metabolism genes was downregulated to a similar extent in *zmnac128 zmnac130 o2*, *zmnac128 zmnac130*, and *o2* (Supplemental Data Set 7). We further performed the immunoblotting assay to detect the protein accumulation of starch metabolism enzymes in 20-DAP endosperms from NT, *o2*, *zmnac128 zmnac130*, and *zmnac128 zmnac130 o2*. Consistent with the previous findings that O2 directly regulates the expression of *SSIII* and *PPDK* (Zhang et al. 2016), these 2 proteins and SSV were reduced in both *o2* and *zmnac128 zmnac130 o2* (Fig. 8E). Zpu1, GBSS1, SS1, Bt2, and SSIIa were reduced in both *zmnac128 zmnac130* and *zmnac128 zmnac130 o2* (Fig. 8E). The protein accumulation of more starch metabolism enzymes was lower in *zmnac128 zmnac130 o2* than in *zmnac128 zmnac130* or *o2*. Therefore, the 2 NACs and O2 separately regulated the expression of different starch metabolism genes. This could be one major cause for the relatively low amount of starch metabolism in *zmnac128 zmnac130 o2*.

Regulation of sugar and nutrient transport from maternal to filial tissue: ZmNAC128, ZmNAC130, and O2 regulate the expression of key transporter genes in the BETL

Our RNA in situ hybridization results showed that *ZmNAC128* and *ZmNAC130* are expressed not only in the SE but also in the BETL (Fig. 9A). This suggested that the 2 NACs possibly regulate the expression of nutrient transfer-related genes in the BETL. To date, 2 sugar transporters (ZmSWEET4c and ZmSUGCAR1, which are also responsible for K^+ uptake), one cell wall invertase (ZmMN1), and one zinc transporter (ZmYSL2) have been characterized as playing crucial roles in mother-to-endosperm transport in the BETL (Cheng et al. 1996; Sosso et al. 2015; Guan et al. 2020; He et al. 2021; Zhou et al. 2021; Wei et al. 2021; Chao et al. 2022; Yang et al. 2022a).

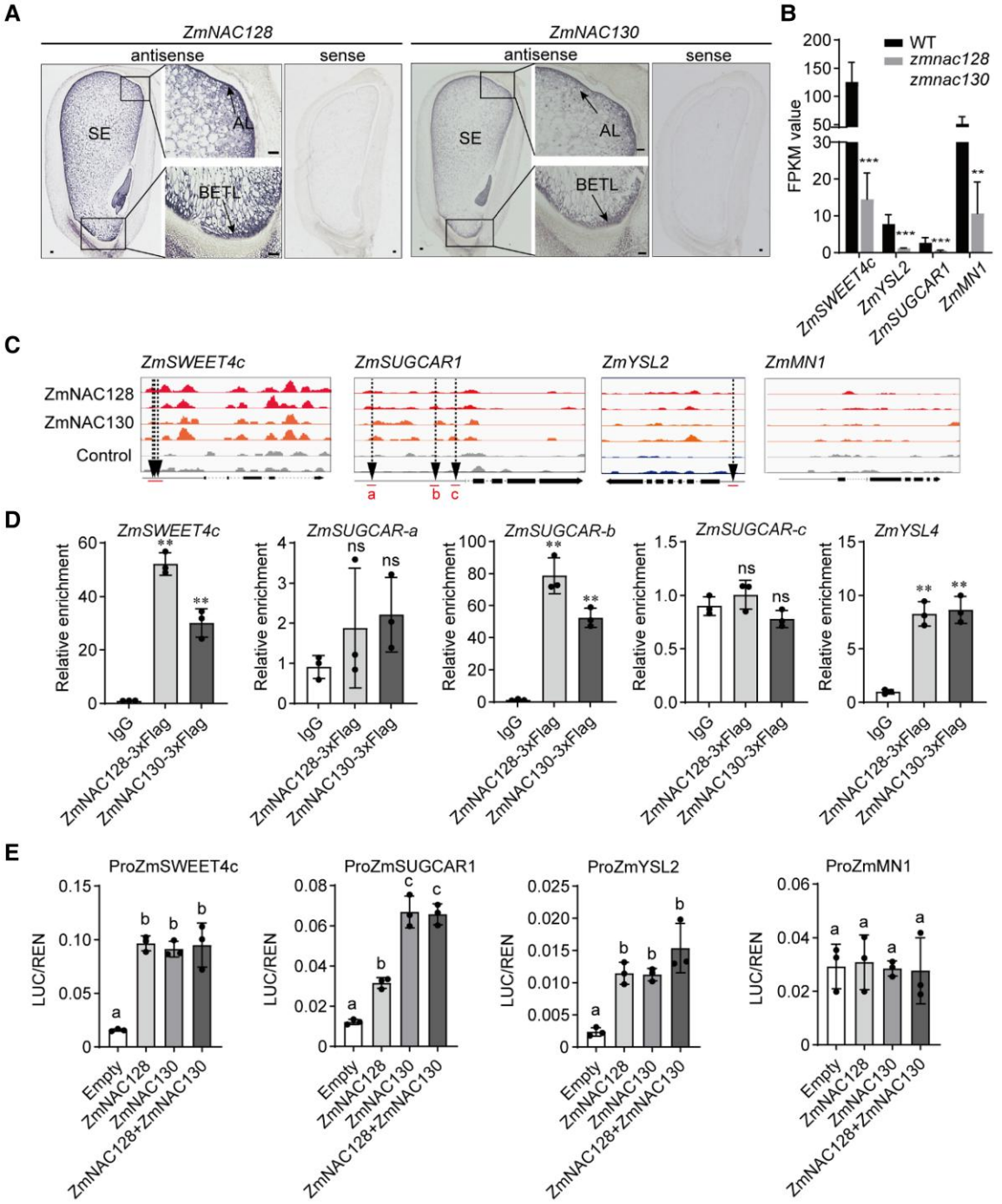

Figure 9. ZmNAC128 and ZmNAC130 regulate the expression of *ZmSWEET4c*, *ZmSUGCAR1*, and *ZmYSL2*. **A)** RNA in situ hybridization of *ZmNAC128* and *ZmNAC130* in 12-DAP B73 kernels. Antisense probes were used to detect the spatial expression of *ZmNAC128* and *ZmNAC130* transcripts. Sense probes were the negative controls. SE, starchy endosperm; AL, aleurone; BETL, basal endosperm transfer layer. Scale bars, 100 μm. **B)** Expression levels of *ZmSWEET4c*, *ZmSUGCAR1*, *ZmYSL2*, and *ZmMN1* in the 16-DAP endosperms of *zmnac128 zmnac130* versus WT in the KN5585 background. Expression levels are shown as FPKM (fragments per kilobase of exon per million mapped reads). Statistical significance was determined by DESeq2R. $^{**}P < 0.01$; $^{***}P < 0.001$. **C)** IGV shows the peaks bound by ZmNAC128 and ZmNAC130 in the 4 promoters. The relative positions of the element GTACGT are marked by arrowheads. **D)** ChIP-qPCR detects the in vivo binding activities of ZmNAC128 and ZmNAC130 to the promoters of *ZmSWEET4c*, *ZmSUGCAR1*, and *ZmYSL2*. The red lines under the arrowheads in **(C)** indicate the region detected by ChIP-qPCR. Data represent means ± SD of 3 independent samples for each test. Statistical significance was determined by a Student's *t*-test. $^{**}P < 0.01$; ns, not significant. **E)** DLR detects the transactivation activities of ZmNAC128, ZmNAC130, and O2 on the 4 promoters. The data was also shown in Supplemental Fig. S19B combined with the transactivation of O2, ZmNAC128, and ZmNAC130 on the 4 promoters. Data represent means ± SD of 3 independent samples for each test. Different lowercase letters indicate significant differences according to a one-way ANOVA with Tukey's multiple comparisons test ($P < 0.05$).

Transcriptome analysis of the whole 16-DAP endosperms, including the BETL, revealed that the expression of *ZmSWEET4c*, *ZmSUGCAR1*, *ZmYSL2*, and *ZmMN1* was significantly reduced by 8.7-, 7.2-, 6.2-, and 4.8-fold in *zmnac128 zmnac130* compared to the WT, respectively (Fig. 9B). DAP-seq analysis indicated that there are peaks corresponding to regions bound by ZmNAC128 and ZmNAC130 in the promoters of *ZmSWEET4c* and *ZmSUGCAR*, but not in the promoters of *ZmMN1* and *ZmYSL2* (Fig. 9C). We further found the cis-element GTACGT consistently around the peak binding regions in the *ZmSWEET4c* and *ZmSUGCAR1* promoters (Fig. 9C). The ChIP-qPCR results confirmed the binding of ZmNAC128 and ZmNAC130 to the 2 promoters (Fig. 9D). We found 3 GTACGT motifs in the *ZmSUGCAR1* promoter, whereas ZmNAC128 and ZmNAC130 recognized only the second motif-containing region (Fig. 9D).

Typically, the protein–DNA interactions could be disrupted by the flanking DNA sequence around the binding motif. For instance, there are 2 ACGCAA elements within a 1,000 bp region of the *Bt2* promoter upstream from the start codon, but ZmNAC128 and ZmNAC130 recognize only the one near the start codon (Zhang et al. 2019). Although our DAP-seq analysis did not find the peaks bound by ZmNAC128 and ZmNAC130 in the *ZmYSL2* promoter, ChIP-qPCR showed the interaction of ZmNAC128 and ZmNAC130 with the GTACGT-centered fragment in the *ZmYSL2* promoter (Fig. 9D). This result suggested that our DAP-seq might have missed some targets. We finally performed DLR assays to detect the transactivation of ZmNAC128 and ZmNAC130 on these 4 promoters. Indeed, ZmNAC128 or ZmNAC130 significantly enhanced the LUC activities driven by the promoters of *ZmSWEET4c*, *ZmSUGCAR1*, and *ZmYSL2* but not by the *ZmMN1* promoter, while their LUC activities were not higher upon co-expression of ZmNAC128 and ZmNAC130 (Fig. 9E).

In view of the more severe endosperm-filling defect of *zmnac128 zmnac130 o2*, we also investigated whether O2 is involved in the regulation of the 4 genes (*ZmSWEET4c*, *ZmSUGCAR1*, *ZmYSL2*, and *ZmMN1*). Transcriptome analysis showed that the expression of only *ZmYSL2* was significantly downregulated twofold in *o2*, although the expression of all 4 genes was downregulated in *zmnac128 zmnac130 o2* (Supplemental Fig. S19A). DLR results indicated that O2 could enhance LUC activities driven by the promoters of *ZmSWEET4c* and *ZmSUGCAR1*. Meanwhile, ZmNAC128 and ZmNAC130 together with O2 could further enhance the transactivation activities driven by the promoters of *ZmSWEET4c*, *ZmSUGCAR1*, and *ZmYSL2* (Supplemental Fig. S19B). Taken together, these results suggested that O2 and the 2 NACs synergistically co-activate these 3 transporter-encoding genes.

Combined effects of these three TFs on sugar and nutrient uptake

To detect whether the mutations of the 3 core TFs affect kernel nutrient uptake, we measured the contents of soluble sugars and elements transported by ZmSWEET4c, ZmSUGCAR1, and ZmYSL2 in the mature dry kernels of the NT, *o2*, *zmnac128 zmnac130*, and *zmnac128 zmnac130 o2*. The levels of soluble sugars (glucose, fructose, and sucrose) in the kernels could be affected by multiple factors, including BETL-related uptake ability and carbohydrate metabolism and accumulation. The levels of glucose, fructose, and sucrose were significantly increased in the kernels of *o2* compared to the NT (Fig. 10A). These results are consistent with those corresponding to the previous determination of soluble sugars in *o2* kernels (Zhang et al. 2016), which is related to decreased starch biosynthesis. However, although starch accumulation is lower in *zmnac128 zmnac130* than *o2*, the levels of soluble sugars are also lower in *zmnac128 zmnac130*.

In particular, the sucrose level is significantly decreased in *zmnac128 zmnac130* compared to the NT, which is similar to the effects that occur when *ZmSUGCAR1* is mutated (Yang et al. 2022a, 2022b). Conversely, the levels of these 3 soluble sugars are much higher in *zmnac128 zmnac130 o2* than *zmnac128 zmnac130* and *o2*, which is similar to what occurs in mutants due to the blockage of starch biosynthesis. This reflects the importance of the 3 core filling TFs in starch synthesis. Although the evaluation of sugar uptake is relatively complex, the loss-of-function mutations of *ZmNAC128* and *ZmNAC130* indeed affect kernel sugar uptake, especially for sucrose.

ZmSUGCAR1 and ZmYSL2 can transport K and Zn from maternal to endosperm respectively, so element analysis was also performed on the mutant kernels. Although there was no statistically significant change in the K level between *zmnac128 zmnac130* and the NT, a significant reduction in the K level was observed in *zmnac128 zmnac130* compared to *o2*.(Fig. 10A). The mutation of *ZmNAC128* and *ZmNAC130* affects the expression of *ZmSUGCAR1* and in turn its transport ability for K and sucrose. The level of Zn, but not Fe, is significantly decreased in *zmnac128 zmnac130* compared to the NT and *o2*. This is consistent with the fact that ZmYSL2 is responsible for the uptake of Zn rather than Fe (Chao et al. 2022), while the Zn level was observed to be even lower in *zmnac128 zmnac130 o2* than *zmnac128 zmnac130* (Fig. 10A).

Overall, O2, ZmNAC128, and ZmNAC130 affect the uptake of soluble sugars, Zn, and K potentially partly through the regulation of the expression of *ZmSWEET4c*, *ZmSUGCAR1*, and *ZmYSL2* (Fig. 10B). By itself, O2 seems to have a very weak effect on the uptake of these nutrients, but it can enhance the function together with ZmNAC128 and ZmNAC130 to affect the transport abilities of ZmSWEET4c, ZmSUGCAR1, and ZmYSL2.

Discussion

The molecular basis of the genetic redundancy between *ZmNAC128* and *ZmNAC130*

ZmNAC128 and *ZmNAC130* are a pair of duplicated genes that arose from the allotetraploidization of maize (Zhang et al. 2019). The previous study suggested the functional redundancy of ZmNAC128 and ZmNAC130 because they regulate the expression of the same downstream genes (*16-kD*

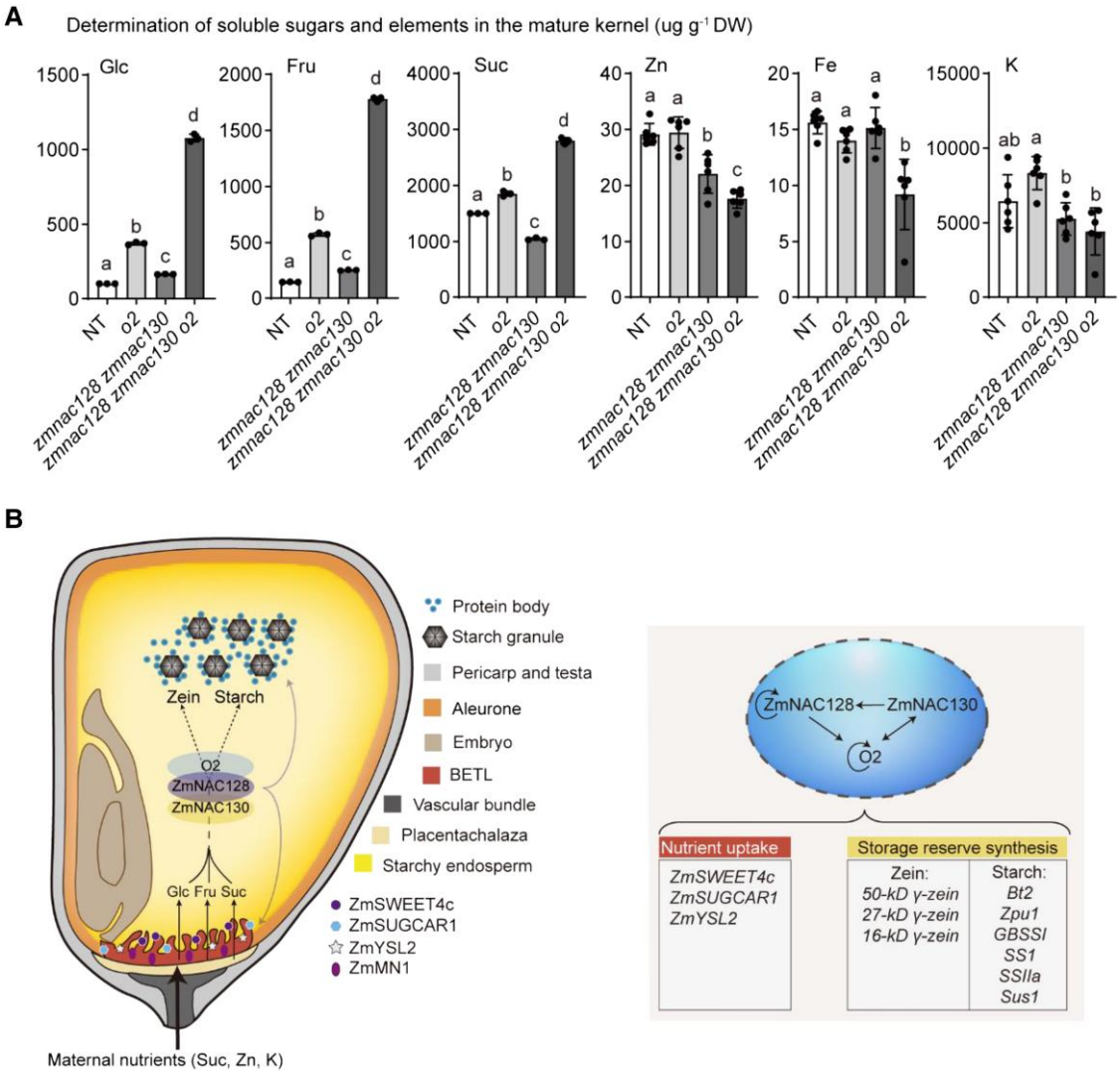

Figure 10. Mutations in *O2*, *ZmNAC128*, and *ZmNAC130* influence soluble sugar and element levels in kernels, and a working model of these 3 TFs facilitates endosperm filling. **A)** Determination of soluble sugars (glucose, fructose, and sucrose) and elements (Zn, Fe, and K) in the mature kernels of NT, *o2*, *zmnac128 zmnac130*, and *zmnac128 zmnac130 o2* in the KN5585 × B73 background. Data represent means ± SD of 3 independent samples in sugar measurement and 6 independent samples in element measurement for each genotype. Different lowercase letters indicate significant differences according to a one-way ANOVA with Tukey's multiple comparisons test ($P < 0.05$). **B)** A working model of O2, ZmNAC128, and ZmNAC130 facilitates endosperm filling. Left panel, a cartoon illustration depicts the cooperation of the 3 TFs to promote endosperm filling. Maternal nutrients are transported via the BETL into the starchy endosperm for synthesis and deposition of storage reserves (starch and zeins). Right panel, the major targets of ZmNAC128 and ZmNAC128 have been characterized in this study except for *16-kD γ-zein* and *Bt2* which have been previously investigated (Zhang et al. 2019). Arrows indicate direct transcriptional regulation.

γ-zein and *Bt2*) by recognizing a common binding motif ACGCAA (Zhang et al. 2019). This study demonstrated the genetic redundancy of ZmNAC128 and ZmNAC130 by generating their knockout mutations. It is generally accepted that the 2 copies of duplicated genes can be retained by functional divergence or stronger functions (such as robustness) in the evolution (Huang et al. 2023). Undoubtedly, ZmNAC128 and ZmNAC130 commonly exert stronger functions in endosperm filling.

ZmNAC128 and ZmNAC130 shared high sequence similarities in both NAC and transactivation domains (Zhang et al. 2019), hinting at their similarities in structure and function. Indeed, the single mutations of *ZmNAC128* and *ZmNAC130* have little effect on the transcriptome (such as a few DEGs) of filling endosperm, but their double mutant leads to thousands of DEGs. Protein–protein interaction experiments also indicated that these 2 NACs can form homo- or hetero-dimer. So when one NAC is absent, the other NAC can form a homodimer to function in filling endosperms. DLR assays were used to assess which kind of interaction exerts stronger functions, either homo- or hetero-dimerization. With the addition of *16-kD γ-zein* and

Bt2 (Zhang et al. 2019), the total 14 direct downstream genes of ZmNAC128 and ZmNAC130 have been verified by their promoter transactivation. In general, the co-expression of ZmNAC128 and ZmNAC130 does not have stronger transactivation in many of these promoters than either of them alone, indicating that the 2 kinds of dimers have roughly equivalent abilities to activate the expression of their target genes.

On the other hand, although the single mutants *zmnac128* and *zmnac130* have no visible kernel phenotypes, their kernel starch contents are slightly reduced compared to the WT. It suggests that the absence of one NAC seems to have a weak effect on their dimerization or polymerization in endosperm cells. Indeed, the co-expression of O2, ZmNAC128, and ZmNAC130 exhibited the highest transactivation activities on the promoters of many of their common target genes in all combinations. And according to the interaction of O2, ZmNAC128, and ZmNAC130, it is supported that ZmNAC128 and ZmNAC130 should form a heterodimer and interact with other cofactors (such as O2) to more effectively regulate complex endosperm filling (Fig. 10B).

O2, ZmNAC128, and ZmNAC130 coordinate the synchronized biosynthesis of zeins and starch

The regulation of zein gene expression during endosperm filling has been comprehensively investigated (Dai et al. 2021; Yang et al. 2023). This study further broadens the understanding of the transcriptional regulation of zein gene expression. Unlike other TFs regulating the expression of zein genes, ZmNAC128 and ZmNAC130 specifically regulate the expression of all 3 (*16-*, *27-*, and *50-kD*) *γ-zein* genes and mediate the expression of other zein genes. However, with the exception of that of 16-kD γ-zein, the accumulation of other zein proteins is not apparently reduced in *zmnac128 zmnac130*. This is very similar to the regulatory ability of O2 on the expression of zein family genes. Although O2 regulates the expression of most zein genes (excluding *16-kD γ-zein*) (Li et al. 2015; Zhan et al. 2018), the accumulation of only α-zeins is apparently reduced in *o2*. The 2 NACs and O2 are the major regulators of the expression of *16-kD γ-zein* and *α-zein*, respectively, while they have minor effects on the regulation of other zein gene expression.

Although the protein accumulation of O2 is largely reduced in *zmnac128 zmnac130*, α-zein accumulation is not apparently reduced in this mutant. This suggested that partial expression of *O2* is sufficient to activate the expression of *α-zein* genes, while other TFs also possibly compensate for the reduction of O2 in *zmnac128 zmnac130*. In addition, all 3 TFs can transactivate the expression of the *27-kD γ-zein* gene, although the accumulation of the 27-kD γ-zein protein is not apparently reduced in the triple mutant. Indeed, multiple TFs have been characterized to regulate the expression of *27-kD γ-zein* (Pysh et al. 1993; VicenteCarbajosa et al. 1997; Wu and Messing 2012; Li et al. 2015; Zhang et al. 2015; Li et al. 2018), supporting the idea that 27-kD γ-zein is essential for PB formation and endosperm filling. The other TFs thus could compensate for the absence of O2, ZmNAC128, and ZmNAC130. Nevertheless, most zein proteins are almost undetectable in *zmnac128 zmnac130 o2*, demonstrating the core function of these 3 TFs in the regulation of zein synthesis.

Moreover, ZmNAC128 and ZmNAC130 directly regulated the expression of at least 6 important starch metabolism genes. The transcript and protein levels of other major starch metabolism genes were also reduced to varying degrees in *zmnac128 zmnac130*, indicating that ZmNAC128 and ZmNAC130 are critical TFs for starch metabolism. ZmNAC128 and ZmNAC130 play even more important roles than O2 in the synchronized biosynthesis of zein and starch. In agreement with this notion, compared with *zmnac128 zmnac130*, *zmnac128 zmnac130 o2* showed less accumulation of storage reserves and more poorly filled kernels. Moreover, these 3 TFs have no universally synergistic effect on the expression of their common target genes for the biosynthesis of starch and zeins. Perhaps the accumulation of the 2 major storage components in the endosperm is synergistically regulated through a more complex mechanism by the 3 core TFs, as they modulate the expression of hundreds or thousands of genes, thus imposing hierarchical regulation on other aspects of development.

Regulatory mechanism underlying the high expression of *O2*, *ZmNAC128*, and *ZmNAC130* during the endosperm-filling stage

Although O2 is a well-known core TF in filling endosperm, the mechanism of regulating *O2* expression is rather unclear. Two recent studies demonstrated that *ZmABI19* and *ZmbZIP29* are highly expressed in the early stage of kernel development and play initial roles in grain filling (Yang et al. 2021; Yang et al. 2022b). ZmABI19 initiates the expression of *O2* and *ZmNAC130*, while ZmbZIP29 and ZmABI19 synergistically transactivate the expression of *O2* upon abscisic acid treatment. Because *ZmABI19* and *ZmbZIP29* are expressed during the early stage, they function mainly as initial regulators of *O2* expression. Auto-activation of *O2* may play a role in activating its expression during the filling stage (Lohmer et al. 1991; Yang et al. 2021), but it is difficult to quantify this contribution. This investigation illustrated how ZmNAC128 and ZmNAC130 act as major regulators to control the expression of more than 50% of transcripts and proteins of *O2* across the entire filling stage via direct regulation. Moreover, the transactivation activity of O2 can be further enhanced in the presence of both NACs and O2. Therefore, these 3 TFs clearly play a decisive role in regulating the high expression of *O2* in the endosperm throughout the whole filling stage.

According to this investigation, although O2 also regulates the expression of *ZmNAC130*, it does not appear to be the core regulator for the expression of *ZmNAC128* and *ZmNAC130*. Because the contribution of auto-activation is hard to quantify with respect to the expression of *ZmNAC128* and *ZmNAC130*, their high expression in filling

endosperm needs to be further investigated. Nevertheless, a hierarchical regulatory circuit among these 3 core TFs is a prerequisite for activating their high expression and endosperm filling.

The function of putative orthologs of ZmNAC128 and ZmNAC130 in the grains of other species

Grain filling involves 2 synchronized processes, i.e. maternal-to-filial nutrient transport and storage component synthesis. However, it was previously unknown whether the expression of the genes involved in these 2 distinct processes is coordinated by common TFs. Recent advances in the functional genomics of maize kernels prompted us to investigate the link between nutrient uptake and storage reserve synthesis. For instance, the maize nutrient uptake-related genes *ZmSWEET4c*, *ZmSUGCAR1*, and *ZmYSL2* are partly or specifically expressed in the filling endosperm, which is highly consistent with the expression pattern of genes responsible for the synthesis of starch and zeins. Here, we found that ZmNAC128 and ZmNAC130 regulate the expression of important filling-related genes in both the BETL and the SE, which in turn facilitate nutrient uptake and storage reserve synthesis in the endosperm (Fig. 10B).

There are no reports on the mechanism underlying the coordination of mother-to-endosperm nutrient transfer and storage reserve biosynthesis during grain filling in other cereals, such as rice (*Oryza sativa*) and wheat (*Triticum aestivum*). OsNAC20, OsNAC26, and TaNAC019, which are homologous to ZmNAC128 and ZmNAC130, were recently shown to coordinate the biosynthesis of starch and storage proteins in the endosperm (Liu et al. 2020; Wang et al. 2020; Gao et al. 2021), although it has yet to be tested whether they are involved in nutrient uptake. Based on DEG analysis of the *TaNAC019* mutant (Supplemental Fig. S20), we preliminarily found that the expression of TraesCS6D02G012100 (a homolog of *ZmSWEET4c*) (Sosso et al. 2015) and TraesCSU02G13020 (a homolog of *ZmSUGCAR1*) (Yang et al. 2022a) is significantly downregulated in the *TaNAC019* mutant.

Like maize, wheat also has a typical transfer cell layer that mediates nutrient transfer from the mother plant to the grain. We hypothesize that TaNAC019 might also be involved in the regulation of endosperm nutrient uptake, although this hypothesis needs to be investigated. However, *OsSWEET4c*, *OsNPF7.9*, and *GRAIN INCOMPLETE FILLING1* (*GIF1*) (Wang et al. 2008) were not among the DEGs identified in the double mutant for *OsNAC20* and *OsNAC26*, indicating that their expression is not significantly altered in the mutant. This suggested that OsNAC20 and OsNAC26 are unlikely to be involved in the regulation of nutrient uptake, but this hypothesis also needs to be investigated.

In summary, ZmNAC128 and ZmNAC130 coordinate with O2 to promote endosperm filling, from nutrient uptake in the BETL to the synthesis of starch and zeins in the SE, while regulating their own expression (Fig. 10B). Therefore, our findings greatly broaden our understanding of grain filling and have potential importance for improving grain-filling efficiency in breeding.

Materials and methods

Plant materials and growth conditions

The CRISPR/Cas9-mediated knockout lines of *ZmNAC128* and *ZmNAC130* were generated in the maize (*Zea mays*) KN5585 background by Agrobacterium (*Agrobacterium tumefaciens*)-mediated transformation as previously described (Frame et al. 2011). The T_1 plants were backcrossed to KN5585 and then self-pollinated to produce homozygous knockout lines without the CRISPR/Cas9 cassette, as determined by PCR identification. The 2 loss-of-function mutant lines for *O2* were identified from a EMS-mutagenized maize inbred B73 population. *o2-1* harbors a premature termination codon at the +417 position downstream from the first codon ATG (start codon). *o2-2* is an acceptor splice site mutation at the boundary between the first intron and the second exon. The *o2-1* mutant used in this study was backcrossed twice to the WT B73 and self-pollinated several times. The triple mutant *zmnac128 zmnac130 o2* was generated from an F_2 ear of *zmnac128 zmnac130* ×*o2-1*. The other 3 genotypes, NT, *o2*, and *zmnac128 zmnac130* were also identified from the same F_2 ear. For the transgenic materials of the *27-kD γ-zein* promoter-driving *ZmNAC128* or *ZmNAC130* expression, the 3′ terminus for each gene was linked to a short nucleotide sequence encoding the 3×FLAG tag. The expression cassettes were transformed into the modified binary vector pTF102 with the GFP driven by the *10-kD δ-zein* promoter as the visible selection marker (Wu and Messing 2012). The transgenic lines were also generated in the KN5585 background through Agrobacterium-mediated transformation. All maize materials were planted in the field of Hefei (Anhui Province, China) and Sanya (Hainan Province, China). *Nicotiana benthamiana* plants were cultivated in a chamber maintained at a constant temperature of 21 °C. The humidity level inside the chamber was maintained at 50% to 60%, and the plants were exposed to a 16-h light cycle each day. The primers for construction and genotyping are listed in Supplemental Data Set 8.

Prediction of starch and protein content in the mature kernels

Mature dry kernels were milled into flour and then filtered with a 50-mesh stainless steel screen. The starch and protein content of the milled flour was predicted using a preconstructed calibration model based on MPA-type Fourier transform near-infrared spectrophotometer (Bruker, Germany). The model calibration was based on 30 different varieties of maize flour samples, of which starch and protein content were determined by the Amyloglucosidase-α-Amylase Method (AOAC 996.11) and the Kjeldahl method (Lynch and Barbano 1999), respectively. These sample spectra were collected on the MPA spectrophotometer and the

modeling algorithm was partial least squares regression. The coefficient of determination (R^2) of starch and protein models were 0.826 and 0.984, respectively, and root-mean-square error of cross-validation (RMSECV) values were 0.533 and 0.123, respectively. The mature kernel flour of each material was divided into 4 portions for measurement. To calculate the percentage of starch and protein in a single kernel per genotype, the values were further calculated based on the kernel weight.

Determination of soluble sugars in the mature kernels

The determinations were performed according to the methods previously reported (Deng et al. 2020). 50 mg of different fresh or matured maize endosperm powder were extracted with 2 mL of deionized water. After incubating the tubes for 30 min on ice, the supernatants were moved to a new 2 mL centrifuge tube after centrifugation at 13,000 × *g* for 15 min at 4 °C and then filtered with the 0.22 μm filter. The resulting filtered liquid was diluted tenfold with deionized water for measurement. The determinations were performed on the ion chromatography (ICS5000, Thermo Fisher Scientific) using a CarboPac PA-20 column. The mobile phase consisted of solvent A (deionized water) and solvent B (200 mM NaOH).

Iodine staining starch in the developing endosperm

The 16- and 20-DAP fresh kernels were longitudinally cut in half with a single-edge blade and the cut kernels were placed in the iodine solution (0.3 g of I_2 and 2 g of KI in 100 ml of deionized water in an amber glass bottle to protect from light at room temperature) for 3 min. Immediately, the staining kernels were rinsed with deionized twice, and then observed and photographed under a stereomicroscope (LEICA S9i).

RNA in situ hybridization

The 12-DAP B73 kernels were used for RNA in situ hybridization. cDNA fragments of *ZmNAC128* and *ZmNAC130* were amplified, and their antisense and sense RNA probes were synthesized by in vitro transcription using T7 RNA polymerase with digoxigenin RNA Labeling Mixture (Roche). Tissue processing and in situ hybridization experiments using 10-mm sections were performed according to the methods described previously (Zhang et al. 2015). A light microscope (Leica DM500) was used to observe paraffin-embedded sections of filling-stage kernels.

Element profiling

The elemental analysis was conducted by inductively coupled plasma mass spectrometry (ICP-MS) as previously described (Chao et al. 2022). This analysis was conducted in the mature kernels of *o2*, *zmnac128 zmnac130*, and *zmnac128 zmnac130 o2* as well as the corresponding wild type. Six dry mature kernels of each genotype were ground into powder by a tomized grinder with a grinding tank (material: polytetrafluoroethylene) and beads (material: Jargonia) manufactured by Jingxin Industry Co., Ltd., Shanghai. 2–5 mg of each sample was used for ICP-MS analysis. The elemental content by ICP-MS was measured following the method as previously described (Chao et al. 2022) and all the solid samples were normalized with a heuristic algorithm using the best-measured elements as previously described (Lahner et al. 2003).

Electron- and light-microscope observation

To observe endosperm texture and starch granules of the wild type and mutants, mature kernels were placed in a drying oven at 45 °C for at least 24 h and then cut along the longitudinal axis of the kernel. Subsequently, the endosperm texture and starch granules in the longitudinal section were observed under a scanning electron microscope (ZEISS Gemini SEM 500), following the instructions outlined on the ZEISS Microscopy website (https://www.zeiss.com/microscopy/en/home.html). For kernel phenotype observations, the longitudinal sections of kernels were observed under a stereomicroscope (LEICA S9i).

Protein extraction, polyclonal antibody generation, and immunoblotting assay

Zein and nonzein proteins from endosperm and kernels were extracted as described previously (Zhang et al. 2015). The protein concentration was determined with a Compat-Able protein assay preparation reagent kit and a BCA protein assay kit (Pierce) according to the standard procedures. 10 μg of nonzein proteins in each sample was loaded for immunoblotting assays with the corresponding antibodies as described previously (Zhang et al. 2015). The antibody against the O2 protein was previously generated (Yang et al. 2021). For the production of antibodies against starch metabolism enzymes in this study, their partial cDNAs (encoding 60–200 amino acids) were amplified by PCR and cloned into the pET51b expression vector. The recombinant plasmids were transformed into *Escherichia coli* BL21 Rosetta 2 (DE3) competent cells. Bacteria were grown at 37 °C until the absorbance at 600 nm (OD600) reached 0.6. Protein production was induced with 0.1 mM isopropyl β-D-1-thiogalactopyranoside (IPTG). Bacteria were cultured at 37 °C for an additional 5 h before pelleting by centrifugation at 4,000 × *g*. The fusion protein was purified on a Ni-NTA His Bind Resin (Novagen). The eluted proteins were dialyzed in PBS 5 times, and about 6 mg was sent to Shanghai Orizymes Biotech Company to produce the antibodies. Detailed information on antigens and their efficacy and specificity are in Supplemental Fig. S21 and Table S2.

Protein purification, pull-down, and Co-IP assay

For the pull-down assay, O2 and ZmNAC130 were fused to a GST tag, and ZmNAC128 and ZmNAC130 were fused to a His-TF tag. The encoding plasmids were transformed into *E. coli* Rosetta and recombinant proteins were extracted and purified. GST, GST-ZmNAC128, and GST-ZmNAC130 were incubated with glutathione beads (GE Healthcare) at 4 °C for 2–3 h; the beads were incubated with

His-ZmNAC128 and His-ZmNAC130 at 4 °C for 2 h. After washing and elution, the proteins were separated by SDS-PAGE and subjected to immunoblot analysis with anti-GST (ProteinTech, No. 10000-0-AP, 1:5,000), anti-His (TransGen Biotech, HT501, 1:5,000), and anti-NAC (Shanghai Orizymes Biotech Company, PAB191213, 1:5,000).

For the Co-IP assay, O2, and ZmNAC130 were fused to 3xFlag, and ZmNAC128 and ZmNAC130 were fused to a 6xMyc tag. The encoding plasmids were transformed into Agrobacterium strain GV3101 and co-expressed in *Nicotiana benthamiana* leaves. Total proteins were extracted in IP buffer (150 mM NaCl, 12.7 mM KCl, 25 mM Na_2HPO_4, 0.5 mM KH_2PO_4 1, 10% [v/v] glycerol, 0.01 mM EDTA, 0.05% [v/v] NP-40, 1 mM PMSF, 5 mM DTT, and 1× protease inhibitor cocktail) at 4 °C for 1 h and then incubated with Flag beads (Sigma–Aldrich, M8823-1 mL) at 4 °C for 2–3 h. The beads were washed 3 to 4 times with washing buffer (50 mM Tris–HCl, pH 7.4, 150 mM NaCl, and 0.1% [v/v] NP-40). After washing, the eluted proteins were separated by SDS-PAGE and subjected to immunoblot analysis with anti-Myc (Cell Signaling Technology, 2278S, 1:2,000) and anti-Flag (Sigma–Aldrich, F1804, 1:2,000) antibodies. The above protein bands were visualized using a Tanon-5200 M imaging system. The primers are listed in Supplemental Data Set 8.

BiFC and LCI assays

O2, ZmNAC128, and ZmNAC130 were fused with the N-terminal or C-terminal half of YFP or LUC. The encoding plasmids were transformed into Agrobacterium strain GV3101 and then co-expressed in *N. benthamiana* leaves. YFP fluorescence was visualized using confocal microscopy (ZEISS980; Carl Zeiss). YFP signals were excited at 514 nm, and emission was detected in the range of 520 to 545 nm with an intensity value of approximately 0.5% and a gain value of around 600. For LCI assays, leaf samples were infiltrated with 1× luciferin, and LUC signals were detected using a Tanon-5200 M imaging system. The primers are listed in Supplemental Data Set 8.

RNA extraction and reverse transcription quantitative PCR

Total RNA was extracted from 12-, 16-, 20-, 24-, and 28-DAP endosperm using TRIzol reagent (Invitrogen) and purified with an RNeasy Mini Kit after DNase I digestion (Qiagen). First-strand cDNA was then generated with a SuperScript III First Strand Kit (Invitrogen). RT-qPCR was performed with SYBR Green (Takara) on a CFX (Real-Time PCR Detection System, which is a product developed by Bio-Rad Laboratories) Connect Real-Time PCR system (Bio-Rad) according to the standard operating manual. The comparative CT (ΔΔCT) method was employed for the relative quantification of gene expression (Livak and Schmittgen 2001), with *ACTIN* serving as the reference. The primers are listed in Supplemental Data Set 8.

RNA-seq

The details for RNA-seq were as described previously. Total RNA was extracted from 16-DAP maize kernel endosperm using TRIzol reagent (Invitrogen) according to the manufacturer's instructions. The concentration and quality of total RNA (from 2 or 3 independent groups of endosperms for each genotype) were determined on a NanoDrop 2000/2000c Spectrophotometer. Sequencing libraries were generated by Novogene Co., Ltd. using a NEBNextUltra RNA Library Prep Kit for Illumina (NEB, USA) following the manufacturer's recommendations; index codes were added to attribute sequences to each sample. The index-coded samples were clustered using a HiSeq 4000 PE Cluster Kit (Illumina) according to the manufacturer's instructions. After cluster generation, the libraries were sequenced on an Illumina HiSeq 4000 platform as 150-bp paired-end reads. The clean reads were aligned to the B73 reference genome (RefGen_v5) through the HISAT2 program (Kim et al. 2015). DEGs were identified as meeting the criteria of an absolute value of $\log_2$(FC) >1 and adjusted *P*-value <0.05 by the R package DESeq (Love et al. 2014).

DAP-seq

The in vitro DAP-seq was performed as described previously, with some minor modifications (Allen et al. 2006; O'Malley et al. 2016; Bartlett et al. 2017). Halo-tagged transcription factors (O2, ZmNAC128, and ZmNAC130) and recombinant proteins were produced in a TNT Coupled Wheat Germ Extract System (Promega). Genomic DNA was extracted from 8-, 12-, and 16-DAP maize kernels using a modified cetyltrimethylammonium bromide (CTAB) extraction method, purified with a FastPure Gel DNA Extraction Mini Kit (Vazyme), and sonicated to ∼200-bp fragments. After end-repair and adenylation, the fragmented gDNA was then purified using AMPure XP Beads (Beckman Coulter). The Halo-tagged-TFs and Halo proteins were bound to Magne HaloTag Beads (Promega) and subsequently incubated with the fragmented gDNA library for 1 h on a rotator at room temperature. The beads were then washed 3 times, and the eluted DNA was ligated to an indexed adaptor for sequencing analysis. For peak analysis, the mapped reads and peak files were examined an using integrative genomics viewer. Enriched motifs were identified by MEME motif discovery software (http://meme-suite.org/). The primers are listed in Supplemental Data Set 8.

ChIP-qPCR

The 16-DAP developing endosperms of *ZmNAC128-3×Flag* and *ZmNAC130-3×Flag* transgenic lines were fixed with 1% (v/v) formaldehyde (Sigma) in phosphate buffer as described previously (Yang et al. 2021). Antibodies against 3×Flag peptide (F1804, Sigma) and Rabbit IgG control (Sigma, 12-370) were used for immunoprecipitation. The experimental procedure is the same as described previously (Li et al. 2015; Yang et al. 2021). The immunoprecipitated DNA was used

for qPCR experiments of target DNA fragments which were performed with SYBR Green (Takara) on a CFX Connect Real-Time PCR system (Bio-Rad) according to the standard operating manual. Relative enrichment of target DNA fragments was calculated by analyzing the immunoprecipitated samples of anti-Flag compared to that of anti-IgG. *ACTIN* is the internal reference gene in the detected samples with 3 biological replicates. The primers are listed in Supplemental Data Set 8.

EMSA

Oligonucleotide probes of the *O2* promoter were synthesized and labeled with biotin at the 3′ end with a Biotin 3′ End DNA Labeling Kit (Thermo) according to the standard procedures. Each probe was mixed with purified recombinant protein at 25 °C for 20 min in reaction buffer (20 μL) containing 10× binding buffer, 50% (v/v) glycerol, 100 mM $MgCl_2$, 1 μg/μL poly(dI-dC), 50 mM KCl, and 1% (v/v) NP-40. Biotin-labeled DNA was detected according to the instructions of the LightShift Chemiluminescent EMSA Kit (Thermo). The luminescence was visualized on a Tanon-5200 M imaging system.

DLR assay

Maize protoplasts were prepared from the leaves of 2-wks seedlings of the inbred B73. The protoplast isolation, polyethylene glycol (PEG)-calcium transfection of plasmid DNA, and protoplast culture were described previously (Zhang et al. 2015). The vector pRI101 (Clontech) was used for the expression of *O2*, *ZmNAC128*, and *ZmNAC130* under the control of the 35S promoter. The transient expression vector pGreenII 0800-LUC was used to generate the reporter constructs by cloning the promoters of different target genes upstream of LUC. The LUC/REN activity ratio was measured using a Dual-luciferase Reporter Assay System (Promega). The primers are listed in Supplemental Data Set 8.

Statistical analysis

Data processing of means, standard deviations, and *P*-values was performed with Microsoft Excel (2016): AVERAGE, STDEV.S, and Student's *t*-test, respectively. The one-way ANOVA test in the SPSS software was employed to determine whether there are significant differences among 3 or more groups. Immunoblotting signals in each band were quantified by ImageJ (https://imagej.nih.gov/ij/). The *P*-value and false discovery rate (FDR) of DEGs in the RNA-seq data were calculated by the DESeq2R package (v 1.28.1 with default arguments). The raw data and detailed statistical analysis are in Supplemental Data Set 9.

Accession numbers

ZmNAC128: Zm00001eb126890; *ZmNAC130*: Zm00001eb334180; *O2*: Zm00001eb301570; *16-kD γ-zein*: Zm00001eb099950; *27-kD γ-zein*: Zm00001eb313800; *50-kD γ-zein*: Zm00001eb313790; *Sus1*: Zm00001eb392880; *SSV*: Zm00001eb191890, *Bt2*: Zm00001eb176800; *SSIIa*: Zm00001eb279740; *GBSSI*: Zm00001eb378140; *SS1*: Zm00001eb376100; *Zpu1*: Zm00001eb088740; *SSIII*: Zm00001eb413290; *Sh2*: Zm00001eb159060; *SBEIIb*: Zm00001eb242610; *PPDK1*: Zm00001eb287770; *PPDK2*: Zm00001eb349810; *Sh1*: Zm00001eb374090; *ISA1*: Zm00001eb174590; *Bt1*: Zm00001eb235570; *ZmSWEET4c*: Zm00001eb236810; *ZmSUGCAR1*: Zm00001eb304390; *ZmYSL2*: Zm00001eb248990; *ZmMN1*: Zm00001eb083790; *ACTIN*: Zm00001eb348450. The RNA-seq and DAP-seq data in this article are available from the National Center for Biotechnology Information Gene Expression Omnibus (http://www.ncbi.nlm.nih.gov/geo) under the series entries PRJNA913969 for RNA-seq data and PRJNA914049 for DAP-seq data.

Acknowledgments

Dr. Joachim Messing's legacy lives on through this project, which owes its inception to his visionary leadership and guidance. We also thank Dr. Xiaoduo Lu from the Qilu Normal University for providing *o2* mutants in a EMS-mutagenized maize inbred B73 library, Dr. Jihua Tang and Qiyue Wang from the Henan Agricultural University for the assistance of DAP-seq experiment, and Dr. Chunguang Chen and Yanwen Xiang from the Orizymes Biotechnologies (Shanghai) Co., Ltd. for the assistance of DAP-seq analyses and ChIP experiments.

Author contributions

Z.Z. supervised the project. Z.Z., E.C., J.H., and D.P. designed the experiments and wrote the manuscript. E.C., H.Y., J.H., and D.P. performed the experiments. P.Z., S.P., X.W., J.W., and C.J. assisted with the fieldwork, material sampling, and identification. Z.C. and D.C. measured and analyzed the element levels in the kernels. Z.X. and Y.W. analyzed seed composition. Y.W. helped conduct the project.

Supplemental data

The following materials are available in the online version of this article.

Supplemental Figure S1. CRISPR/Cas9-mediated knockout mutation of *ZmNAC128* and *ZmNAC130*.

Supplemental Figure S2. Venn diagram shows the number of overlapped genes between DAP-seq and DEGs of *zmnac128 zmnac130*.

Supplemental Figure S3. A list of candidate motifs of ZmNAC128 and ZmNAC130 identified by MEME-ChIP.

Supplemental Figure S4. Coomassie Brilliant Blue-staining SDS-PAGE of zein proteins in mature kernels of WT, *zmnac128*, *zmnac130*, and *zmnac128 zmnac130*.

Supplemental Figure S5. Immunoblotting detection of ZmNAC128 and ZmNAC130 proteins in the 16-DAP endosperms of ZmNAC128-3×Flag and ZmNAC130-3×Flag transgenes.

Supplemental Figure S6. IGV shows the distribution of binding peaks in the promoters of some starch metabolism genes.

Supplemental Figure S7. FPKM value of *O2* expression in 16-DAP endosperm transcriptomes of knockdown and knockout mutants of *ZmNAC128* and *ZmNAC130* in different genetic backgrounds.

Supplemental Figure S8. Quantification of O2 protein accumulation in the filling endosperms of *zmnac128 zmnac130* compared to the WT.

Supplemental Figure S9. The competitive EMSA of P3 probes bound by ZmNAC128 and ZmNAC130 using 50× and 200× unlabeled P3 probes.

Supplemental Figure S10. The LCI assay detects the interaction of O2, ZmNAC128, and ZmNAC130.

Supplemental Figure S11. Negative controls of BiFC assay in Fig. 6B.

Supplemental Figure S12. Identification of the 2 EMS-mutagenized *o2* mutant alleles in the B73 background.

Supplemental Figure S13. DLR assay detecting the transactivation activities of O2, ZmNAC128, and ZmNAC130 on the *O2* promoter.

Supplemental Figure S14. O2, ZmNAC128, and ZmNAC130 regulate the expression of *ZmNAC128* and *ZmNAC130*.

Supplemental Figure S15. O2, ZmNAC128, and ZmNAC130 regulate the expression of *MYBR13*.

Supplemental Figure S16. Enrichment analysis of GO terms of the 581 common DEGs in Fig. 8C.

Supplemental Figure S17. DLR assay detects the transactivation activities of O2, ZmNAC128, and ZmNAC130 on the promoters of *27-kD* and *50-kD γ-zein*.

Supplemental Figure S18. Potassium iodide staining of 16-and 20-DAP kernels of NT, *o2*, *zmnac128 zmnac130*, and *zmnac128 zmnac130 o2* in the KN5585 × B73 background.

Supplemental Figure S19. O2, ZmNAC128, and ZmNAC130 regulate the expression of *ZmSWEET4c*, *ZmSUGCAR1*, *ZmYSL2*, and *ZmMN1*.

Supplemental Figure S20. Expression of putative homologous of *ZmSWEET4c* and *ZmSUGCAR1* in wheat mutant *nac019* versus WT.

Supplemental Figure S21. The antigenic information and immunoblotting detection for the corresponding proteins.

Supplemental Table S1. The expression of zein family genes in *zmnac128 zmnac130* versus WT in the KN5585 background.

Supplemental Table S2. The information of antibodies purchased by the Shanghai Orizymes Biotech Company.

Supplemental Data Set 1. Up- and downregulated genes in the 16-DAP endosperm of *zmnac128 zmnac130* versus WT.

Supplemental Data Set 2. Peak distribution of ZmNAC128 and ZmNAC130 in the maize genome.

Supplemental Data Set 3. Identification of NAC-binding peaks within 1 kb regions around TSS for 248 upregulated and 250 downregulated genes in *zmnac128 zmnac130*.

Supplemental Data Set 4. Putative target genes of ZmNAC128 and ZmNAC130.

Supplemental Data Set 5. The expression of genes in the starch metabolism pathway, pentose phosphate pathway, glycolysis, and tricarboxylic acid cycle in *zmnac128 zmnac130* and WT in the KN5585 background.

Supplemental Data Set 6. The expression of zein family genes in NT, *o2*, *zmnac128 zmnac130*, and *zmnac128 zmnac130 o2* in the KN5585 × B73 background.

Supplemental Data Set 7. The expression of genes in starch metabolism pathway, pentose phosphate pathway, glycolysis, and tricarboxylic acid cycle in NT, *o2*, *zmnac128 zmnac130*, and *zmnac128 zmnac130 o2* in the KN5585 × B73 background.

Supplemental Data Set 8. Primers were used in this study.

Supplemental Data Set 9. Detailed statistical analysis in this study.

Funding

This work was supported by the National Natural Science Foundation of China (31671703 and 32072010 to Z.Z.), start-up funding from the University of Science and Technology of China (KY9100000020 and WK9100000017 to Z.Z.), and the Chinese Academy of Sciences (KJ2070000078 to Z.Z.).

Conflict of interest statement. The authors declare to have no conflicts of interest.

References

Allen GC, Flores-Vergara MA, Krasynanski S, Kumar S, Thompson WF. A modified protocol for rapid DNA isolation from plant tissues using cetyltrimethylammonium bromide. Nat Protoc. 2006:**1**(5): 2320–2325. https://doi.org/10.1038/nprot.2006.384

Bartlett A, O'Malley RC, Huang SC, Galli M, Nery JR, Gallavotti A, Ecker JR. Mapping genome-wide transcription-factor binding sites using DAP-seq. Nat Protoc. 2017:**12**(8):1659–1672. https://doi.org/10.1038/nprot.2017.055

Becraft PW, Gutierrez-Marcos J. Endosperm development: dynamic processes and cellular innovations underlying sibling altruism. Wiley Interdiscip Rev Dev Biol. 2012:**1**(4):579–593. https://doi.org/10.1002/wdev.31

Boston RS, Larkins BA. The genetics and biochemistry of maize zein storage proteins. In: **Bennetzen JL, Hake S**, editors. Handbook of maize: genetics and genomics. New York (NY): Springer New York; 2009. p. 715–730.

Chao Z, Chen Y, Ji C, Wang Y, Huang X, Zhang C, Yang J, Song T, Wu J, Guo L, et al. A genome-wide association study identifies a transporter for zinc uploading to maize kernels. EMBO Rep. 2022:**24**(1): e55542. https://doi.org/10.15252/embr.202255542

Chen J, Zeng B, Zhang M, Xie S, Wang G, Hauck A, Lai J. Dynamic transcriptome landscape of maize embryo and endosperm development. Plant Physiol. 2014:**166**(1):252–264. https://doi.org/10.1104/pp.114.240689

Cheng WH, Taliercio EW, Chourey PS. The miniature1 seed locus of maize encodes a cell wall invertase required for normal development of endosperm and maternal cells in the pedicel. Plant Cell. 1996:**8**(6): 971–983. https://doi.org/10.2307/3870209

Chourey PS, Hueros G. The basal endosperm transfer layer(BETL): gateway to the maize kernel. In: **Larkins BA**, editors. Maize kernel development. Boston (MA): CABI; 2017. p. 56–67.

Dai D, Ma Z, Song R. Maize endosperm development. J Integr Plant Biol. 2021:**63**(4):613–627. https://doi.org/10.1111/jipb.13069

Deng Y, Wang J, Zhang Z, Wu Y. Transactivation of Sus1 and Sus2 by opaque2 is an essential supplement to sucrose synthase-mediated endosperm filling in maize. Plant Biotechnol J. 2020:**18**(9): 1897–1907. https://doi.org/10.1111/pbi.13349

Feng F, Qi W, Lv Y, Yan S, Xu L, Yang A, Yuan Y, Chen Y, Zhao H, Song R. OPAQUE11 Is a central hub of the regulatory network for maize endosperm development and nutrient metabolism. Plant Cell. 2018:**30**(2):375–396. https://doi.org/10.1105/tpc.17.00616

Flint-Garcia SA. Kernel evolution: from teosinte to maize. In: **Larkins BA**, editors. Maize kernel development. Boston (MA): CABI; 2017. p. 1–16.

Flint-Garcia SA, Bodnar AL, Scott MP. Wide variability in kernel composition, seed characteristics, and zein profiles among diverse maize inbreds, landraces, and teosinte. Theor Appl Genet. 2009:**119**(6): 1129–1142. https://doi.org/10.1007/s00122-009-1115-1

Frame B, Main M, Schick R, Wang K. Genetic transformation using maize immature zygotic embryos. Methods Mol Biol. 2011:**710**: 327–341. https://doi.org/10.1007/978-1-61737-988-8_22

Galli M, Khakhar A, Lu Z, Chen Z, Sen S, Joshi T, Nemhauser J, Schmitz R, Gallavotti A. The DNA binding landscape of the maize AUXIN RESPONSE FACTOR family. Nat Commun. 2018:**9**(1):4526. https://doi.org/10.1038/s41467-018-06977-6

Gao Y, An K, Guo W, Chen Y, Zhang R, Zhang X, Chang S, Rossi V, Jin F, Cao X, et al. The endosperm-specific transcription factor TaNAC019 regulates glutenin and starch accumulation and its elite allele improves wheat grain quality. Plant Cell. 2021:**33**(3):603–622. https://doi.org/10.1093/plcell/koaa040

Gomez E, Royo J, Guo Y, Thompson R, Hueros G. Establishment of cereal endosperm expression domains: identification and properties of a maize transfer cell-specific transcription factor, ZmMRP-1. Plant Cell. 2002:**14**(3):599–610. https://doi.org/10.1105/tpc.010365

Gomez E, Royo J, Muniz LM, Sellam O, Paul W, Gerentes D, Barrero C, Lopez M, Perez P, Hueros G. The maize transcription factor Myb-related protein-1 is a key regulator of the differentiation of transfer cells. Plant Cell. 2009:**21**(7):2022–2035. https://doi.org/10.1105/tpc.108.065409

Gontarek BC, Neelakandan AK, Wu H, Becraft PW. NKD Transcription factors are central regulators of maize endosperm development. Plant Cell. 2016:**28**(12):2916–2936. https://doi.org/10.1105/tpc.16.00609

Guan H, Dong Y, Lu S, Liu T, He C, Liu C, Liu Q, Dong R, Wang J, Li Y, et al. Characterization and map-based cloning of miniature2-m1, a gene controlling kernel size in maize. J Integr Agric. 2020:**19**(8): 1961–1973. https://doi.org/10.1016/S2095-3119(19)62797-8

Hannah LC, Boehlein S. Starch biosynthesis in maize endosperm. In: **Larkins BA**, editor. Maize kernel development. Boston (MA): CABI; 2017. p. 149–159.

He Y, Yang Q, Yang J, Wang Y, Sun X, Wang S, Qi W, Ma Z, Song R. Shrunken4 is a mutant allele of ZmYSL2 that affects aleurone development and starch synthesis in maize. Genetics. 2021:**218**(2):iyab070. https://doi.org/10.1093/genetics/iyab070

Huang J, Xu W, Zhai J, Hu Y, Guo J, Zhang C, Zhao Y, Zhang L, Martine C, Ma H, et al. Nuclear phylogeny and insights into whole-genome duplications and reproductive development of Solanaceae plants. Plant Commun. 2023:**4**(4):100595. https://doi.org/10.1016/j.xplc.2023.100595

Huang L, Tan H, Zhang C, Li Q, Liu Q. Starch biosynthesis in cereal endosperms: an updated review over the last decade. Plant Commun. 2021:**2**(5):100237. https://doi.org/10.1016/j.xplc.2021.100237

Kim D, Langmead B, Salzberg SL. HISAT: a fast spliced aligner with low memory requirements. Nat Methods. 2015:**12**(4):357–360. https://doi.org/10.1038/nmeth.3317

Lahner B, Gong J, Mahmoudian M, Smith EL, Abid KB, Rogers EE, Guerinot ML, Harper JF, Ward JM, Mcintyre L, et al. Genomic scale profiling of nutrient and trace elements in Arabidopsis thaliana. Nat Biotechnol. 2003:**21**:1215–1221.

Larkins BA, Wu Y, Song R, and Messing J. Maize seed storage proteins. In: **Larkins BA**, editor. Maize kernel development. Boston (MA): CABI; 2017. p. 157–189.

Lending CR, Larkins BA. Changes in the zein composition of protein bodies during maize endosperm development. Plant Cell. 1989:**1**(10):1011–1023. https://doi.org/10.1105/tpc.1.10.1011

Leroux BM, Goodyke AJ, Schumacher KI, Abbott CP, Clore AM, Yadegari R, Larkins BA, Dannenhoffer JM. Maize early endosperm growth and development: from fertilization through cell type differentiation. Am J Bot. 2014:**101**(8):1259–1274. https://doi.org/10.3732/ajb.1400083

Li C, Qiao Z, Qi W, Wang Q, Yuan Y, Yang X, Tang Y, Mei B, Lv Y, Zhao H, et al. Genome-wide characterization of cis-acting DNA targets reveals the transcriptional regulatory framework of opaque2 in maize. Plant Cell. 2015:**27**(3):532–545. https://doi.org/10.1105/tpc.114.134858

Li C, Yue Y, Chen H, Qi W, Song R. The ZmbZIP22 transcription factor regulates 27-kD gamma-zein gene transcription during maize endosperm development. Plant Cell. 2018:**30**(10):2402–2424. https://doi.org/10.1105/tpc.18.00422

Li Q, Wu Y. The encyclopedia of maize kernel gene expression. J Integr Plant Biol. 2020:**62**(7):879–881. https://doi.org/10.1111/jipb.12869

Liu Y, Hou J, Wang X, Li T, Majeed U, Hao C, Zhang X. The NAC transcription factor NAC019-A1 is a negative regulator of starch synthesis in wheat developing endosperm. J Exp Bot. 2020:**71**(19):5794–5807. https://doi.org/10.1093/jxb/eraa333

Livak KJ, Schmittgen TD. Analysis of relative gene expression data using real-time quantitative PCR and the $2-\Delta\Delta CT$ method. Methods. 2001:**25**(4): 402–408. https://doi.org/10.1006/meth.2001.1262

Lohmer S, Maddaloni M, Motto M, Di Fonzo N, Hartings H, Salamini F, Thompson RD. The maize regulatory locus opaque-2 encodes a DNA-binding protein which activates the transcription of the b-32 gene. Embo J. 1991:**10**(3):617–624. https://doi.org/10.1002/j.1460-2075.1991.tb07989.x

Love MI, Huber W, Anders S. Moderated estimation of fold change and dispersion for RNA-seq data with DESeq2. Genome Biol. 2014:**15**(12):550. https://doi.org/10.1186/s13059-014-0550-8

Lynch JM, Barbano DM. Kjeldahl nitrogen analysis as a reference method for protein determination in dairy products. J AOAC Int. 1999:**82**(6):1389–1398. https://doi.org/10.1093/jaoac/82.6.1389

Ning L, Wang Y, Shi X, Zhou L, Ge M, Liang S, Wu Y, Zhang T, Zhao H. Nitrogen-dependent binding of the transcription factor PBF1 contributes to the balance of protein and carbohydrate storage in maize endosperm. Plant Cell. 2022:**35**(1):409–434. https://doi.org/10.1093/plcell/koac302

O'Malley RC, Huang SC, Song L, Lewsey MG, Bartlett A, Nery JR, Galli M, Gallavotti A, Ecker JR. Cistrome and epicistrome features shape the regulatory DNA landscape. Cell. 2016:**166**(6):1598. https://doi.org/10.1016/j.cell.2016.08.063

Olsen OA. ENDOSPERM DEVELOPMENT: cellularization and cell fate specification. Annu Rev Plant Physiol Plant Mol Biol. 2001:**52**(1): 233–267. https://doi.org/10.1146/annurev.arplant.52.1.233

Pysh LD, Aukerman MJ, Schmidt RJ. OHP1: a maize basic domain/leucine zipper protein that interacts with opaque2. Plant Cell. 1993:**5**(2): 227–236. https://doi.org/10.1105/tpc.5.2.227

Qiao Z, Qi W, Wang Q, Feng Y, Yang Q, Zhang N, Wang S, Tang Y, Song R. ZmMADS47 regulates zein gene transcription through interaction with Opaque2. PLoS Genet. 2016:**12**(4):1005991. https://doi.org/10.1371/journal.pgen.1005991

Sabelli PA, Larkins BA. The development of endosperm in grasses. Plant Physiol. 2009:**149**(1):14–26. https://doi.org/10.1104/pp.108.129437

Schmidt RJ, Burr FA, Aukerman MJ, Burr B. Maize regulatory gene opaque-2 encodes a protein with a leucine-zipper motif that binds to zein DNA. Proc Natl Acad Sci U S A. 1990:**87**(1):46–50. https://doi.org/10.1073/pnas.87.1.46

Schmidt RJ, Burr FA, Burr B. Transposon tagging and molecular analysis of the maize regulatory locus opaque-2. Science. 1987:**238**(4829): 960–963. https://doi.org/10.1126/science.2823388

Sosso D, Luo D, Li Q, Sasse J, Yang J, Gendrot G, Suzuki M, Koch KE, McCarty DR, Chourey PS, et al. Seed filling in domesticated maize and rice depends on SWEET-mediated hexose transport. Nat Genet. 2015:**47**(12):1489–1493. https://doi.org/10.1038/ng.3422

VicenteCarbajosa J, Moose SP, Parsons RL, Schmidt RJ. A maize zinc-finger protein binds the prolamin box in zein gene promoters and interacts with the basic leucine zipper transcriptional activator Opaque2. Proc Natl Acad Sci U S A. 1997:**94**(14):7685–7690. https://doi.org/10.1073/pnas.94.14.7685

Wang E, Wang J, Zhu X, Hao W, Wang L, Li Q, Zhang L, He W, Lu B, Lin H, et al. Control of rice grain-filling and yield by a gene with a potential signature of domestication. Nat Genet. 2008:**40**(11): 1370–1374. https://doi.org/10.1038/ng.220

Wang J, Chen Z, Zhang Q, Meng S, Wei C. The NAC transcription factors OsNAC20 and OsNAC26 regulate starch and storage protein synthesis. Plant Physiol. 2020:**184**(4):1775–1791. https://doi.org/10.1104/pp.20.00984

Wei Y, Ren Z, Wang B, Zhang L, Zhao Y, Wu J, Li L, Zhang X, Zhao X. A nitrate transporter encoded by ZmNPF7.9 is essential for maize seed development. Plant Sci. 2021:**308**:110901. https://doi.org/10.1016/j.plantsci.2021.110901

Wu Y, Messing J. Rapid divergence of prolamin gene promoters of maize after gene amplification and dispersal. Genetics. 2012:**192**(2): 507–519. https://doi.org/10.1534/genetics.112.142372

Wu Y, Holding DR, Messing J. gamma-Zeins are essential for endosperm modification in quality protein maize. Proc Natl Acad Sci U S A. 2010:**107**(29):12810–12815. https://doi.org/10.1073/pnas.1004721107

Xin M, Yang R, Li G, Chen H, Laurie J, Ma C, Wang D, Yao Y, Larkins BA, Sun Q, et al. Dynamic expression of imprinted genes associates with maternally controlled nutrient allocation during maize endosperm development. Plant Cell. 2013:**25**(9):3212–3227. https://doi.org/10.1105/tpc.113.115592

Yang B, Wang J, Yu M, Zhang M, Zhong Y, Wang T, Liu P, Song W, Zhao H, Fastner A, et al. The sugar transporter ZmSUGCAR1 of the nitrate transporter 1/peptide transporter family is critical for maize grain filling. Plant Cell. 2022a:**34**(11):4232–4254. https://doi.org/10.1093/plcell/koac256

Yang T, Guo L, Ji C, Wang H, Wang J, Zheng X, Xiao Q, Wu Y. The B3 domain-containing transcription factor ZmABI19 coordinates expression of key factors required for maize seed development and grain filling. Plant Cell. 2021:**33**(1):104–128. https://doi.org/10.1093/plcell/koaa008

Yang T, Wang H, Guo L, Wu X, Xiao Q, Wang J, Wang Q, Ma G, Wang W, Wu Y. ABA-induced phosphorylation of basic leucine zipper 29, ABSCISIC ACID INSENSITIVE 19 and Opaque2 by SnRK2.2 enhances gene transactivation for endosperm filling in maize. Plant Cell. 2022b:**34**(5):1933–1956. https://doi.org/10.1093/plcell/koac044

Yang T, Wu X, Wang W, Wu Y. Regulation of seed storage protein synthesis in monocot and dicot plants: a comparative review. Mol Plant. 2023:**16**(1):145–167. https://doi.org/10.1016/j.molp.2022.12.004

Yi F, Gu W, Chen J, Song N, Gao X, Zhang X, Zhou Y, Ma X, Song W, Zhao H, et al. High temporal-resolution transcriptome landscape of early maize seed development. Plant Cell. 2019:**31**(5):974–992. https://doi.org/10.1105/tpc.18.00961

Zhan J, Dannenhoffer JM, Yadegari R. Endosperm development and cellspecialization. In: **Larkins BA**, editors. Maize kernel development. Boston (MA): CABI; 2017. p. 28–43.

Zhan J, Li G, Ryu CH, Ma C, Zhang S, Lloyd A, Hunter BG, Larkins BA, Drews GN, Wang X, et al. Opaque-2 regulates a complex gene network associated with cell differentiation and storage functions of maize endosperm. Plant Cell. 2018:**30**(10):2425–2446. https://doi.org/10.1105/tpc.18.00392

Zhan J, Thakare D, Ma C, Lloyd A, Nixon NM, Arakaki AM, Burnett WJ, Logan KO, Wang D, Wang X, et al. RNA Sequencing of laser-capture microdissected compartments of the maize kernel identifies regulatory modules associated with endosperm cell differentiation. Plant Cell. 2015:**27**(3):513–531. https://doi.org/10.1105/tpc.114.135657

Zhang Y, Liu T, Meyer CA, Eeckhoute J, Johnson DS, Bernstein BE, Nusbaum C, Myers RM, Brown M, Li W, et al. Model-based analysis of ChIP-seq (MACS). Genome Biol. 2008:**9**(9):R137. https://doi.org/10.1186/gb-2008-9-9-r137

Zhang Z, Dong J, Ji C, Wu Y, Messing J. NAC-type transcription factors regulate accumulation of starch and protein in maize seeds. Proc Natl Acad Sci U S A. 2019:**116**(23):11223–11228. https://doi.org/10.1073/pnas.1904995116

Zhang Z, Yang J, Wu Y (2015). Transcriptional regulation of zein gene expression in maize through the additive and synergistic action of opaque2, prolamine-box binding factor, and O2 heterodimerizing proteins. Plant Cell **27**(D), 1162–1172. doi:10.1105/tpc.15.00035

Zhang Z, Zheng X, Yang J, Messing J, Wu Y. Maize endosperm-specific transcription factors O2 and PBF network the regulation of protein and starch synthesis. Proc Natl Acad Sci U S A. 2016:**113**(39): 10842–10847. https://doi.org/10.1073/pnas.1613721113

Zhou L, Liu C, Chen Q, Wang W, Yao S, Zhao Z, Zhu S, Hong X, Xiong Y, Cai Y. Fine mapping and candidate gene analysis of maize defective kernel mutant dek54. Acta Agron Sin. 2021:**47**(10):1903–1912. https://doi.org/10.3724/SP.J.1006.2021.03060